DOI: 10.1093/jnci/djr190
Advance Access publication on June 17, 2011.

ARTICLE

Novel Effect of Antihelminthic Niclosamide on S100A4-Mediated Metastatic Progression in Colon Cancer

Ulrike Sack, Wolfgang Walther, Dominic Scudiero, Mike Selby, Dennis Kobelt, Margit Lemm, Iduna Fichtner, Peter M. Schlag, Robert H. Shoemaker, Ulrike Stein

Manuscript received April 30, 2010; revised April 28, 2011; accepted May 2, 2011.

Correspondence to: Ulrike Stein, PhD, Experimental and Clinical Research Center, Charité University Medicine at the Max-Delbrück-Center for Molecular Medicine, Robert-Rössle-St 10, 13125 Berlin, Germany (e-mail: ustein@mdc-berlin.de).

Background Metastasis formation in colon cancer severely reduces the survival rate in patients. S100A4, a calcium-binding protein, is implicated in promoting metastasis formation in colon cancer.

Methods To identify a transcription inhibitor of S100A4, high-throughput screening of 1280 pharmacologically active compounds was performed using a human colon cancer cell line expressing a S100A4 promoter–driven luciferase (LUC) reporter gene construct (HCT116-S1004p-LUC). Niclosamide, an antihelminthic agent, was identified as a potential candidate. Colon cancer cell lines (HCT116, SW620, LS174T, SW480, and DLD-1) were treated with 1 μM niclosamide to analyze the effect on S100A4 mRNA and protein expression by quantitative reverse transcription–polymerase chain reaction and immunoblot assays, and effects on cell migration, invasion, proliferation, and colony formation were also assessed in vitro. The effect of niclosamide on liver metastasis was assessed in a xenograft mouse model of human colon cancer (n = 8 mice) by in vivo imaging. The long-term effect of niclosamide on metastasis formation after discontinued treatment was quantified by scoring, and overall survival (n = 12 mice) was analyzed by Kaplan–Meier method after discontinuation of treatment. All statistical tests were two-sided.

Results Reduced S100A4 mRNA and protein expression, and inhibited cell migration, invasion, proliferation, and colony formation were observed in niclosamide-treated colon cancer cells in vitro. In vivo imaging of niclosamide-treated mice showed reduced liver metastasis compared with solvent-treated control mice (n = 4 mice per group). Compared with the control group, discontinuation of treatment for 26 days showed reduced liver metastasis formation in mice (n = 6 mice per group) (control vs discontinuous treatment, mean metastasis score = 100% vs 34.9%, mean difference = 65.1%; 95% confidence interval [CI] = 18.4% to 111.9%, $P < .01$) and increased overall survival (n = 6 mice per group; control vs discontinuous treatment, median survival = 24 vs 46.5 days, ratio = 0.52, 95% CI = 0.19 to 0.84, $P = .001$).

Conclusion Niclosamide inhibits S100A4-induced metastasis formation in a mouse model of colon cancer and has therapeutic potential.

J Natl Cancer Inst 2011;103:1018–1036

Colon cancer is one of the most frequent causes of cancer death worldwide. Despite intensive health-care programs for early diagnosis of colon cancer, the majority of patients are still diagnosed at an advanced stage of the disease (1). Progression of colon cancer is particularly associated with metastasis formation. Patients with nonmetastatic, local stage I tumors have a 5-year survival rate of 90%. However, this rate drastically drops to approximately 10% when distant metastases have formed at the time of diagnosis (2). Because metastases remain a major problem in cancer treatment, many efforts were made to identify the molecular pathways regulating target genes that promote metastasis formation. The canonical wingless-type MMTV integration site family (WNT)/catenin β1 (CTNNB1; also known as β-catenin) signaling pathway is deregulated in about 90% of colon tumors leading to constitutively active expression of target genes (3). One major target that is linked to metastasis formation is S100 calcium binding protein A4 (S100A4), a 11 kDa molecular weight protein that was originally identified as metastasin 1 (MTS1) (4).

S100A4 is overexpressed in many different types of cancer such as gallbladder, bladder, breast, esophageal, gastric, pancreatic, hepatocellular, non–small cell lung, and especially colorectal cancer (5). Increased expression of S100A4 is strongly associated with aggressiveness of a tumor, its ability to metastasize, and poor survival in patients (5–7). However, S100A4 itself is not tumorigenic because transgenic mice overexpressing S100A4 do not develop tumors per se (8). But, when S100A4 transgenic mice are crossed

with mice demonstrating spontaneous tumor formation, it leads to aggressive tumor growth and metastasis (8,9). Moreover, S100A4-null mice injected with highly metastatic mouse mammary carcinoma cells show no metastases (10). These observations suggest that S100A4 is essential for the process of metastasis formation.

S100A4 plays a major role in cellular processes such as migration, invasion, adhesion, and angiogenesis, which form the basis for metastasis formation (11). For example, S100A4 increases cell motility by interacting with proteins from the cytoskeleton, such as the myosin, heavy chain 9, non-muscle (MYH9) (12–14). Moreover, S100A4 participates in cell adhesion by interaction with protein tyrosine phosphatase receptor type F (PTPRF) interacting protein, binding protein 1 (PPFIBP1; also known as liprin β-1) and promotes cell invasion and angiogenesis via upregulation of matrix metallopeptidases (MMPs) (15–19).

Despite intensive research revealing the manifold roles of S100A4, no inhibitor of S100A4 expression has been described thus far that inhibits S100A4-mediated metastasis. In this study, we report a high-throughput screening of 1280 small molecules to identify inhibitors of S100A4 promoter–driven reporter gene expression with potential clinical antimetastatic activity. Niclosamide, an approved antihelminthic drug for treatment of tapeworm infections, was identified as a potential candidate. We validated the inhibitory effect of niclosamide on S100A4 expression and elucidated its effects on constitutively active WNT/CTNNB1 signaling pathway. We then examined the effects of niclosamide on S100A4-induced cell migration and invasion as well as cell proliferation and colony formation in vitro. Moreover, we analyze the antimetastatic potential of niclosamide in a metastatic colon cancer mouse xenograft model.

CONTEXT AND CAVEATS

Prior knowledge

The 5-year survival rate drops from 90% in patients with nonmetastatic colon cancer to 10% in metastatic colon cancer. S100A4, a calcium binding protein, is associated with promoting metastasis formation.

Study design

A high-throughput screening of the Library of Pharmacologically Active Compounds 1280 for inhibitors of S100A4 expression was performed. Niclosamide, an antihelminthic drug, was identified as a potential candidate. The effect of the drug was tested on S100A4-induced migration, invasion, proliferation, and colony formation of human colon cancer cells in vitro and metastasis formation in vivo in a mouse xenograft model.

Contribution

Treatment with niclosamide showed reduced S100A4 expression and inhibition of S100A4-mediated cell migration and invasion, but cell proliferation and colony formation were independent of S100A4 expression in vitro. Liver metastasis was inhibited in the mouse model.

Implications

Niclosamide has the potential for the clinical treatment or prevention of colon cancer metastasis in humans.

Limitations

Niclosamide was administered intraperitoneally in tumor-bearing mice. Because this drug is given orally to treat patients with helminthosis, it is not known whether oral administration of niclosamide will still show antimetastatic effect. This study in a mouse model may not necessarily translate to clinical benefits in humans.

From the Editors

Materials and Methods

Cell Lines and Cell Culture

Human colon cancer cell lines HCT116, SW620, LS174T, SW480, and DLD-1 were all grown in RPMI-1640 medium (PAA Laboratories, Pasching, Austria) supplemented with 10% fetal bovine serum (FBS; Invitrogen, Carlsbad, CA). The human glioma cell line U251 was grown in RPMI-1640 medium supplemented with 5% FBS. HCT116 cells were previously described to be heterozygous for the deletion mutation of codon 45 in one of the two CTNNB1 alleles resulting in the loss of serine 45, which is the initial phosphorylation site in CTNNB1 protein needed for proteasomal degradation (4,20). This mutation is therefore a gain-of-function mutation leading to a constitutively active CTNNB1-induced target gene transcription. Homologous recombination was used to either delete the wild-type CTNNB1 allele resulting in the HCT116-derivative cell clone, HAB-68^{mut}, or to delete the mutated CTNNB1 allele resulting in the HCT116-derivative cell clone, HAB-92^{wt} (20). Both cell clones were kindly provided by Dr Todd Waldman (Georgetown University, Washington, DC). All cells were expanded briefly in culture and cryopreserved in multiple replicate vials. These cell banks were tested by PCR and culture methods and found to be free of mycoplasma. To authenticate the cell lines, short tandem repeat genotyping was performed in August 2010 using the ABI Identifier Kit (Applied Biosystems, Carlsbad, CA). All cells were maintained in a humidified incubator at 37°C and 5% CO_2.

Monoclonal and Polyclonal Antibodies

The monoclonal mouse anti-human CTNNB1 antibody and the monoclonal mouse anti-human tubulin-β1 (TUBB1) antibody were both purchased from BD Biosciences (Heidelberg, Germany). The monoclonal mouse anti-human proliferating cell nuclear antigen (PCNA) antibody was purchased from Cell Signaling Technologies (Danvers, MA). The polyclonal rabbit anti-human S100A4 antibody was purchased from Dako (Glostrup, Denmark). The polyclonal goat anti-human glyceraldehyde-3-phosphate dehydrogenase (GAPDH) antibody and the horseradish peroxidase (HRP)-conjugated anti-goat antibody were purchased from Santa Cruz Biotechnology (Santa Cruz, CA). HRP-conjugated anti-rabbit was purchased from Promega (Madison, WI). HRP-conjugated anti-mouse IgG and anti-mouse IgM were purchased from Invitrogen.

Cloning and Stable Transfections of HCT116 Cells

A plasmid carrying the S100A4 promoter sequence (−1487 bp upstream to +33 bp downstream of the S100A4 transcription start site) was kindly provided by Dr David Allard (Peninsula Medical School, University of Exeter and University of Plymouth, Exeter,

UK). The plasmid was digested with *Kpn*I and *Hind*III restriction enzymes (Fermentas, St Leon-Rot, Germany), and the promoter was cloned into the pGL1.4 vector (Invitrogen) to obtain a construct with the firefly luciferase (LUC) reporter gene under the control of S100A4 promoter and with a neomycin resistance cassette (21). HCT116 cells were transfected with this construct and selected for neomycin resistance to generate HCT116-S100A4p-LUC cells. A plasmid carrying the S100A4 cDNA sequence was kindly provided by Dr Claus Heizmann (University of Zurich, Zurich, Switzerland) (22). The plasmid was digested with *Hind*III and *Xba*I restriction enzymes (Fermentas), and S100A4 cDNA was cloned into the pcDNA3.1 vector containing a puromycin resistance. HCT116 cells were transfected with this construct to generate HCT116-S100A4 cells or with the empty pcDNA3.1 vector to obtain HCT116-vector cells. We also amplified the LUC reporter gene by PCR (forward primer, 5′-TGCGGATCCATGGAAGAT GCCAAAAACATTAAGAA-3′; reverse primer, 5′-TACGAATT CTTACACGGCGATCTTGCCG-3′). The PCR conditions were as follows: 94°C for 2 minutes; 40 cycles of 94°C for 30 seconds, 60°C for 30 seconds, and 72°C for 30 seconds; 72°C for 5 minutes. The PCR product was cloned into pcDNA3.1 vector under the control of cytomegalovirus (CMV) promoter at the restriction sites *Bam*HI and *Eco*RI. HCT116 cells were transfected with this construct to generate HCT116-CMVp-LUC cells. All cloned constructs were sequenced by Invitek (Berlin, Germany) for correct in-frame orientation. All stable transfections were performed with Metafectene (Biontex Laboratories, Munich, Germany), according to the manufacturer's instructions. Transfected cells were selected with 1 mg/mL neomycin (PAA Laboratories) or 1 μg/mL puromycin (Invitrogen).

High-Throughput Screening

For high-throughput screening, HCT116-S100A4p-LUC cells (2.5×10^3 cells per well) were seeded into white opaque 384-well plates (PerkinElmer, Waltham, MA) using the BIOMEK 2000 automatic pipetting system (Beckman Coulter, Brea, CA). All 1280 compounds of the Library of Pharmacologically Active Compounds (LOPAC 1280) obtained from Sigma-Aldrich (St Louis, MO) were dissolved initially in dimethylsulfoxide (DMSO) and then diluted in RPMI-1640 culture medium. Samples of test compounds were then added to assay plates containing cells that were treated for 24 hours with each compound at concentrations of 0.1, 1, 10, and 100 μM (single well per concentration). Following treatment with compounds, luciferase expression was determined using Britelite reagent (PerkinElmer) in a Wallac Victor reader (PerkinElmer). In parallel, cytotoxicity of the compounds was measured in clear polystyrene 384-well Corning Costar plates (Costar, Cambridge, MA) by Alamar blue cytotoxicity assay (Sigma-Aldrich). After treatment with compounds for 24 hours, cells were treated with Alamar blue dissolved in serum-free RPMI-1640 and incubated for 4 hours. To measure the fluorescent Alamar blue metabolite, which is generated by dye reduction in viable cells, plates were then read on a Wallac Victor reader (PerkinElmer) at an excitation wavelength of 530 nm and emission wavelength of 590 nm. For both luminescence and Alamar blue fluorescence data, an average of eight control wells treated with DMSO was calculated, and results of test compounds (single well) were expressed as percent of control. The concentrations effective in reducing luciferase activity or Alamar blue fluorescence by 50% were derived from concentration–response curves by linear interpolation. The Alamar blue vs luciferase activity ratio representing toxicity vs activity ratio (≥2.0) was used to identify and prioritize S100A4 inhibitors least likely to be because of cytotoxicity. In addition, as a selectivity screen, inhibitory compounds were also analyzed based on their ability to inhibit hypoxia-inducible factor 1, alpha subunit (basic helix-loop-helix transcription factor) (HIF1A)–driven or constitutive luciferase reporter expression in U251 glioma cells (23) used in a previous high-throughput screen of LOPAC. Compounds showing the best evidence for selective reporter inhibition not because of toxicity were then subjected to detailed concentration–response testing in both assays using duplicate wells per concentration and 20 twofold dilutions from a starting concentration of 100 μM.

Drugs and Treatments

Niclosamide (2′,5-dichloro-4′-nitrosalicylanilide) was obtained from Sigma-Aldrich. Niclosamide derivatives were obtained from the Drug Synthesis and Chemistry Branch, Developmental Therapeutics Program, National Cancer Institute (Bethesda, MD). All drugs were solubilized in DMSO for in vitro application. For in vivo application, niclosamide was administered as suspension in 10% Cremophor EL (BASF, Ludwigshafen, Germany) and 0.9% NaCl solution. Control mice were treated with the appropriate volume of solvent solution (10% Cremophor EL and 0.9% NaCl).

Quantitative Reverse Transcription–Polymerase Chain Reaction (qRT-PCR)

HCT116, SW620, LS174T, SW480, or DLD-1 cells (4×10^5) were plated in six-well plates, and after 24 hours total RNA was isolated from the cells using Trizol Reagent (Invitrogen), according to the manufacturer's instructions. Quantification of RNA concentration was performed with Nanodrop (Peqlab, Erlangen, Germany), and 50 ng total RNA was reverse transcribed with random hexamers in a reaction mix (10 mM $MgCl_2$, 1× RT-buffer, 250 μM pooled dNTPs, 1 U/μL RNAse inhibitor, 2.5 U/μL Moloney Murine Leukemia Virus reverse transcriptase; all from Applied Biosystems). Reaction occurred at 42°C for 15 minutes, 99°C for 5 minutes, and subsequent cooling at 5°C for 5 minutes. The cDNA product was amplified in a total volume of 10 μL in 96-well plates using the LightCycler 480 (Roche Diagnostics, Mannheim, Germany) and the following PCR conditions: 95°C for 10 minutes, followed by 45 cycles of 95°C for 10 seconds, 61°C for 30 seconds, and 72°C for 4 seconds. For S100A4 cDNA quantification, the following primer and probes were used: forward primer, 5′-CTCAGCGCTTC TTCTTTC-3′; reverse primer, 5′-GGGTCAGCAGCTCCTT TA-3′; fluorescein isothiocyanate probe, 5′-TGTGATGGTG TCCACCTTCCACAAGT-3′; and LCRed640-probe, 5′- TCGG GCAAAGAGGGTGACAAGT-3′. For cDNA quantification of the housekeeping gene glucose-6-phosphate dehydrogenase (G6PD), the LightCycler-h-G6PDH Housekeeping Gene Set (Roche Diagnostics) was used, according to manufacturer's instructions. Data analysis was performed with LightCycler 480 Software release 1.5.0 SP3 (Roche Diagnostics). Mean values were calculated from duplicate qRT-PCR reactions. Each mean value of the

expressed gene was normalized to the respective mean amount of the G6PD cDNA. All experiments were performed at least three independent times.

Protein Extraction and Immunoblot

For total protein extraction, HCT116, SW620, LS174T, SW480, or DLD-1 cells (4×10^5) were plated in six-well plates, and after 24 hours the cells were lysed with RIPA buffer (50 mM Tris–HCl [pH 7.5], 150 mM NaCl, 1% Nonidet P-40, supplemented with complete protease inhibitor tablets; Roche Diagnostics) for 30 minutes on ice. For isolation of the nuclear protein fraction, the NE-PER Nuclear and Cytoplasmic Extraction Kit (Pierce, Rockford, IL) was used according to the manufacturer's instructions. Protein concentration was quantified with Bicinchoninic Acid Protein Assay Reagent (Pierce), according to manufacturer's instructions, and lysates of equal protein concentration were separated with sodium dodecyl sulfate-polyacrylamide gel electrophoresis (SDS-PAGE) and transferred to Hybond C Extra nitrocellulose membranes (GE Healthcare, Munich, Germany). Membranes were incubated in blocking solution containing 5% nonfat dry milk and 1% bovine serum albumin for 1 hour at room temperature. Membranes were incubated overnight at 4°C with rabbit anti-human S100A4 antibody (dilution, 1:1500), mouse anti-human CTNNB1 antibody (dilution, 1:1000), mouse anti-human TUBB1 antibody (dilution, 1:1000), goat anti-human GAPDH antibody (dilution, 1:500), or mouse anti-human PCNA antibody (dilution, 1:1000) followed by incubation for 1 hour at room temperature with HRP-conjugated anti-goat IgG (dilution, 1:10 000), anti-rabbit IgG (dilution, 1:10 000), anti-mouse IgG (dilution, 1:10 000), or anti-mouse IgM (dilution, 1:10 000) antibody. Antibody-protein complexes were visualized with electrochemical luminescence reagent (100 mM Tris–HCl, 0.025% wt/vol luminol, 0.011% wt/vol para-hydroxycoumaric acid, 10% vol/vol dimethylsulfoxide, 0.004% vol/vol H_2O_2, pH 8.6) and subsequent exposure to CL-XPosure Films (Pierce) for 1 second to 20 minutes. Immunoblotting for GAPDH and PCNA served as protein loading control. Immunoblotting for TUBB1 was used to control that nuclear extracts were free from cytoplasmatic protein. All experiments were performed at least three independent times.

Boyden Chamber Transwell Migration and Invasion Assay

HCT116, SW620, LS174T, SW480, and DLD-1 cells were used in cell migration and invasion analysis was performed with Boyden chamber assay. Cells (2.5×10^5) in 400 µL RPMI-1640 medium were seeded into each transwell chamber with filter membranes of 12.0 µm pore size (Millipore, Schwalbach, Germany). For invasion, filter membranes were coated with 50 µL Matrigel (BD Biosciences) (diluted 1:3 in RPMI-1640) 10 minutes before cells were seeded. Fresh medium (600 µL) was added to the bottom chamber and cells were allowed to attach to the insets for 15 hours. Both chambers were treated with 1 µM niclosamide or the respective volume of DMSO and incubated at 37°C and 5% CO_2 in a humidified incubator for 24 hours. Afterward, insets were removed and cells that had migrated through the membrane to the lower chamber were incubated in trypsin–EDTA and counted 10 times in Neubauer chambers (LO-Laboroptik, Bad Homburg, Germany). Each migration or invasion experiment was performed in duplicate. The average number of migrated or invaded cells was determined from at least three independent experiments.

Wound Healing Assay

For wound healing assays, HCT116, SW620, LS174T, SW480, and DLD-1 cells were grown to form cell monolayers of 60% confluency in which a wound of approximately 300 µm width was inflicted with a sterile pipette tip. The culture medium was exchanged to remove nonadherent cells, and the wounded monolayer was treated with 1 µM niclosamide or the respective amount of DMSO every 24 hours for 4 consecutive days. The progress of wound closure (healing) was monitored with microphotographs of ×10 magnification taken with the Leica DM IL light microscope (Leica Microsystems, Wetzlar, Germany) on days 1 and 4. The wound healing experiment was performed three independent times.

Anchorage-Dependent Cell Proliferation

For cell proliferation assays, HCT116, SW620, LS174T, SW480, and DLD-1 cells (2×10^3) were seeded in 96-well plates (one plate for each day) and incubated for 24 hours to allow the cells to attach to the bottom of the wells. Cells were then treated daily with 1 µM niclosamide or the respective volume of DMSO. For determination of viable cells, 3-(4,5-dimethyl-2-thiazol)-2,5-diphenyl-2H-tetrazolium bromide (MTT; Sigma-Aldrich) was added to a final concentration of 0.5 mg/mL and incubated for 3 hours at 37°C and 5% CO_2 in a humidified incubator. MTT was reduced to purple formazan crystals by the mitochondria of living cells, and the increase in metabolized MTT reflected the increase in the number of cells. Crystallized MTT was resolved by 10% SDS in 10 mM HCl, and the absorption was measured at 560 nm. MTT measurements were performed daily for five consecutive days. The mean metabolized MTT concentration was determined from two independent experiments, each performed in triplicate.

Colony Formation Assay

Analysis of anchorage-independent cell proliferation was achieved by soft agar colony formation assay. To form a bottom layer, we added 2 mL 0.5% wt/vol agarose, RPMI-1640 medium, 10% FBS, and 1 µM niclosamide or the respective volume of DMSO, to a 6 cm culture dish and incubated at room temperature under sterile conditions for 10 minutes. On the solidified bottom layer, a top layer containing HCT116, SW620, LS174T, SW480, or DLD-1 cells (8×10^3 cells in 0.33% wt/vol agarose, RPMI-1640 medium, 10% FBS, and 1 µM niclosamide or the respective volume of DMSO) was added. Cells were seeded as single cells into the soft agar and incubated in a humidified incubator at 37°C and 5% CO_2 for 7 days. Colony formation was visualized by ×10 magnification for an overview and ×40 magnification for single colonies in the Leica DM IL light microscope (Leica Microsystems). Only colonies with more than four cells were counted in 10 squares of 1 μm^2. Colony formation experiments were repeated two independent times, each in triplicate.

Reporter Assay for WNT/CTNNB1 Pathway Activity

The lymphoid enhancer–binding factor 1 (LEF)/transcription factor (TCF) activity reporter assay, also known as TOPflash/FOPflash assay (Promega), was previously used to analyze the WNT/CTNNB1 pathway activity in human colon cancer cells (24). The assay comprises the TOPflash plasmid, which contains a hexameric repetition of the LEF/TCF-binding element upstream of a thymidine kinase (TK) promoter, and firefly luciferase as

reporter gene. The FOPflash plasmid contains the exact sequence of the TOPflash plasmid but with point mutated LEF/TCF-binding sites. In the assay, HCT116 cells (8×10^4) were plated in 24-well plates and were incubated for 15 hours to allow the cells to attach to the bottom of the dish before transfection. Cells were transfected with TOPflash or FOPflash plasmids using Metafectene, according to the manufacturer's instructions. After 24 hours, they were treated with 1 μM niclosamide or the respective volume of DMSO for another 24 hours. Luciferase activity, which was measured for LEF/TCF activity and thus WNT/CTNNB1 pathway activity, was measured by using the Steady Glow Luciferase Assay System (Promega), according to the manufacturer's instructions, in the luminescence reader SpectraFluor Plus (Tecan, Crailsheim, Germany) with 1500 milliseconds exposure time and a gain of 150. TOPflash reporter gene expression (representing the WNT pathway activity) was normalized to FOPflash reporter gene expression (representing basal reporter gene expression and transfection efficiency). The average activity was calculated from three independent experiments, each in duplicate.

Electrophoretic Mobility Shift Assay (EMSA)

EMSA was performed as previously described (4). Briefly, HCT116 cells (5×10^6) were plated into a 10 cm culture dish and incubated for 15 hours to allow the cells to attach to the bottom of the dish. Cells were treated with 0.1, 0.3, 0.6, or 1 μM niclosamide or the respective volume of DMSO for 24 hours. For each condition, 5 μg nuclear extracted protein was incubated for 30 minutes at room temperature with 0.05% wt/vol poly(deoxyinosinic-deoxycytidylic) acid sodium salt, 0.5 mM Tris, 0.05 mM EDTA, 2.5% vol/vol glycerol, 0.2% vol/vol Nonidet P-40, 5 mM $MgCl_2$, and double-stranded biotinylated oligonucleotides (forward, 5′-CCGGGCATGGGGATCCCCACCCCAGTTTTTGTTTCTGAATCTTTATTTTTTTAAGAGACA-3′ and reverse, 3′-GGCCCGTACCCCTAGGGGTGGGGTCAAAAACAAAGA CTTAGAAATAAAAAAATTCTCTGT-5′) encompassing the TCF-binding site of the S100A4 promoter. For supershift assay, 1.25 μg monoclonal mouse anti-human CTNNB1 antibody was added. Electrophoretic separation of the protein–oligonucleotide complexes was performed in precast Novex 6% tris-borate-EDTA (TBE) gels (Invitrogen) and in TBE buffer (45 mM Tris, 45 mM boric acid, 1 mM EDTA, pH 8.3) for 60 minutes at 100 V. Capillary transfer of the protein–oligonucleotide complexes to the Hybond-N nylon membrane (Amersham Biosciences, Freiburg, Germany) occurred in 20× saline–sodium citrate buffer (3 M NaCl, 300 mM sodium citrate, pH 7.0) overnight. Cross-linkage of transferred DNA to the membrane occurred at 250 mJ/cm^2 for 1 minute in the FL-20-M FluoLink Crosslinker (Bachofer, Reutlingen, Germany). Visualization of biotin-labeled DNA was performed with LightShift Chemiluminescent EMSA Kit (Pierce), according to manufacturer's instructions. Two independent experiments were performed.

Chromatin Immunoprecipitation (ChIP)

ChIP were performed as previously described to determine the binding of CTNNB1 protein to the S100A4 promoter (4). For the preparation of cell lysates, HCT116 cells (1×10^6) were plated in 10 cm culture dish 15 hours before cells were treated with 1 μM niclosamide or the respective volume of DMSO for 24 hours. Cells were incubated with 1% formaldehyde for 10 minutes at room temperature to allow reversible cross-linking of proteins and DNA. Cells were washed twice with ice-cold phosphate buffered saline (PBS) and lysed with lysis buffer (1% SDS, 10 mM EDTA, 50 mM Tris–HCl, pH 8.0) for 10 minutes on ice. Cell lysates were sonicated for 20 pulses at 40% output and centrifuged at 10 000*g* for 10 minutes. Supernatant was transferred to a new tube and one-third of the diluted supernatant was stored at −20°C and served in the end as input control. For immunoprecipitation, the diluted supernatant was incubated with 5 μg monoclonal mouse anti-human CTNNB1 antibody or 5 μg control IgG overnight at 4°C. Protein G beads (Invitrogen) were added and incubated for 2 hours at 4°C. Unbound protein was washed away twice with wash buffer A (10 mM Tris, 0.1% SDS, 0.1% Na-deoxycholate, 1% Triton X-100, 1 mM EDTA, 0.5 mM EGTA, 140 mM NaCl, pH 8.0), once with wash buffer B (wash buffer A, 6% wt/vol NaCl) and twice with TE buffer (20 mM Tris, 1 mM EDTA, pH 8.0). Protein–DNA complex was eluted from the beads by incubation with 1.5% wt/vol SDS solution for 15 minutes at room temperature followed by centrifugation at 1000*g* for 1 minute. To assure complete elution, a second elution step was performed by incubation of the beads in 0.5% SDS solution for 15 minutes at room temperature followed by centrifugation at 1000*g* for 1 minute. Cross-linking was reversed at 68°C for 4 hours, and residual protein was digested by proteinase K (Fermentas) at 55°C for 2 hours. DNA was purified by precipitation, and PCR amplification of the S100A4 promoter TCF-binding site (forward primer 5′-TGTTCCCCTCCAGATCCC-3′; reverse primer 5′-GGCTATGCTCAAGCCACTG-3′) was performed. PCR amplification of the non–CTNNB1-regulated FBJ murine osteosarcoma viral oncogene homolog (FOS) promoter sequence (forward primer 5′-CCTTAATATTCCCACACATGGC-3′; reverse primer 5′-CTGCGTTTGGAAGCAGAAAGT-3′) was used as a control. The expected amplicons for S100A4 and FOS were 167 or 149 bp in size, respectively. ChIP was performed two independent times.

In Vivo Luminescence Imaging of Metastasis Formation

All experiments were performed in accordance with the United Kingdom Coordinated Committee on Cancer Research (UKCCCR) guidelines and approved by the responsible local authorities (State Office of Health and Social Affairs, Berlin, Germany). HCT116-CMVp-LUC cells (3×10^6 cells per mouse, resuspended in 50 μL PBS) were intrasplenically transplanted into 6-week-old female non obese diabetic–severe combined immunodeficiency (NOD-SCID) mice (n = 53). The intrasplenic transplantation and the random assignment of mice to groups were done by two independent researchers. For in vivo imaging (n = 8 mice), mice were randomly assigned to two groups (n = 4 mice per group). Mice were treated 24 hours after transplantation intraperitoneally daily with 10 mL/kg solvent solution (10% Cremophor EL; 0.9% NaCl) or 20 mg/kg niclosamide in solvent. For luminescence imaging, mice were anesthetized with 35 mg/kg Hypnomidate (Janssen-Cilag, Neuss, Germany) and received intraperitoneally 150 mg/kg D-luciferin (Biosynth, Staad, Switzerland) dissolved in sterile PBS. Imaging was performed with the NightOWL LB 981 system (Berthold Technologies, Bad Wildbad, Germany) with exposure times of

1 and 20 seconds. ImageJ version 2.3 (Freeware) was used for color coding of signal intensity (presenting a 256 grayscale) and overlay pictures. For quantification of liver metastases, mice bearing xenograft tumors (n = 27 mice) were randomly assigned to three groups, and treatment of mice started 24 hours after HCT116-CMVp-LUC cell transplantation. Mice in the control group (n = 9 mice) were treated intraperitoneally daily with 10 mL/kg solvent solution. Mice in the second group (n = 9 mice) were treated intraperitoneally daily with 20 mg/kg niclosamide. Mice in the third group (n = 9 mice) were treated intraperitoneally twice daily with 15 mg/kg niclosamide per dose. The experimental endpoint was reached when mice appeared moribund and/or the spleen tumor was palpable. This was the case with the majority of control mice on day 24. Spleen (as the transplantation site) and liver (as a metastasis target organ) were removed. RNA was isolated from tumor cryosections using Trizol Reagent (Invitrogen), as described earlier. The amount of S100A4 mRNA in the tumor was detected by qRT-PCR. The level of metastasis was evaluated by scoring. The score for each liver was calculated as the sum of the volumes of the individual metastasis. Tumor volume (mm^3) was calculated as ($L \times W^2$), where L = length (mm) and W = width (mm).

For long-term in vivo experiments, xenografted mice (n = 18) were randomly assigned to three groups. Mice in the control group (n = 6 mice) were treated intraperitoneally daily with 10 mL/kg solvent solution. Mice in the second group (n = 6 mice) were treated intraperitoneally daily with 20 mg per kg niclosamide. Mice in the third group (n = 6 mice) were treated intraperitoneally daily for 24 days with 20 mg/kg niclosamide and for the residual days with 10 mL/kg solvent solution. Mice were killed by cervical dislocation when tumor reached the maximum size, in accordance with the local authorities. In vivo imaging of mice was performed on the endpoint as described above. Spleen and liver were removed. Liver metastases were quantified by scoring as described above. Organs were shock frozen in liquid nitrogen, and on day 50 total mRNA was isolated from all tumors as described above. The S100A4 expression was quantified by qRT-PCR.

Statistical Analysis

All calculations and statistical analyses were performed with GraphPad Prism version 4.01 (GraphPad Sofware Inc, La Jolla, CA). Student *t* test was used for comparison of only two groups. One-way analysis of variance was applied for comparing the control group with several treated groups followed by Bonferroni post hoc multiple comparisons. In cell cytotoxicity assays, the half-maximal effective concentration (EC_{50}) at which the cell viability was reduced to 50% was calculated by sigmoidal dose–response curve fit of $x = \log(x)$ transformed data, where x represents the concentration of niclosamide. Kaplan–Meier analysis was used to plot overall survival and differences in curves were analyzed by log-rank test. All tests were two-sided, and *P* values less than .05 were considered to be statistically significant.

Results

High-Throughput Screening for S100A4 Inhibitors

HCT116-S100A4p-LUC colon cancer cells stably expressing a human S100A4 promoter–driven luciferase (LUC) reporter gene construct (Figure 1, A) were used to screen the LOPAC 1280, which represents a collection of 1280 well-characterized small molecule inhibitors. In an initial screening using four concentrations (0.1, 1, 10, and 100 μM) of each compound, we identified 34 compounds that inhibited S100A4 promoter–driven luciferase expression by greater than 50% compared with solvent-treated

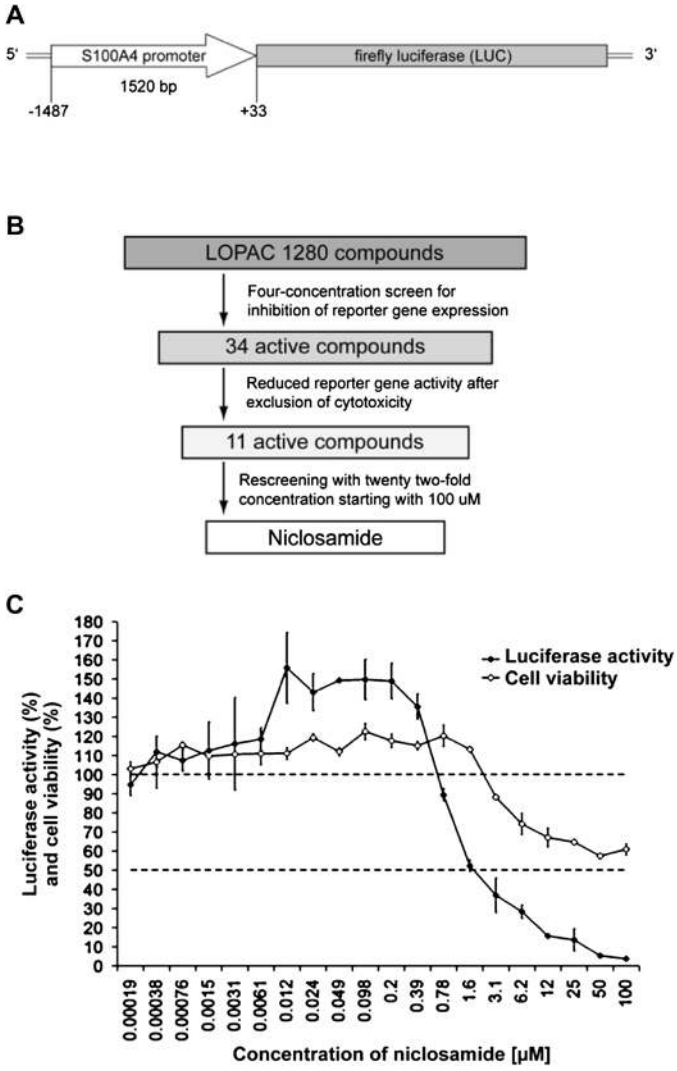

Figure 1. Identification of S100A4 transcription inhibitor via high-throughput screening. **A**) Schematic representation of the reporter system used in high-throughput screening. The expression of reporter firefly luciferase (LUC) was regulated by the S100A4 promoter (−1487 bp upstream to +33 bp downstream of the S100A4 transcription start site). **B**) Schematic representation of high-throughput screening. S100A4 promoter (S100A4p)-LUC construct was stably expressed in HCT116 cells (HCT116-S100A4p-LUC), and cells were treated with 1280 compounds of the Library of Pharmacologically Active Compounds. Four dilutions per compound (100, 10, 1, and 0.1 μM) were tested in the four-concentration screen. Of the 34 compounds that inhibited reporter gene activity, 11 did not reduce cell viability by greater than 50% and were rescreened. **C**) Rescreening with serial dilutions of niclosamide. HCT116-S100A4p-LUC cells were treated with 20 twofold serial dilutions of niclosamide for 24 hours, starting with 100 μM concentration. Luciferase activity was determined using Britelite reagent, and cell viability was measured using Alamar blue cytotoxicity assay. The means (**solid and open circles**) and SD (**vertical lines**) of duplicate samples from one independent experiment are presented. The **horizontal dashed lines** represent 100% cell viability and the half-maximal effective concentration (EC_{50}) at which the cell viability was reduced to 50%.

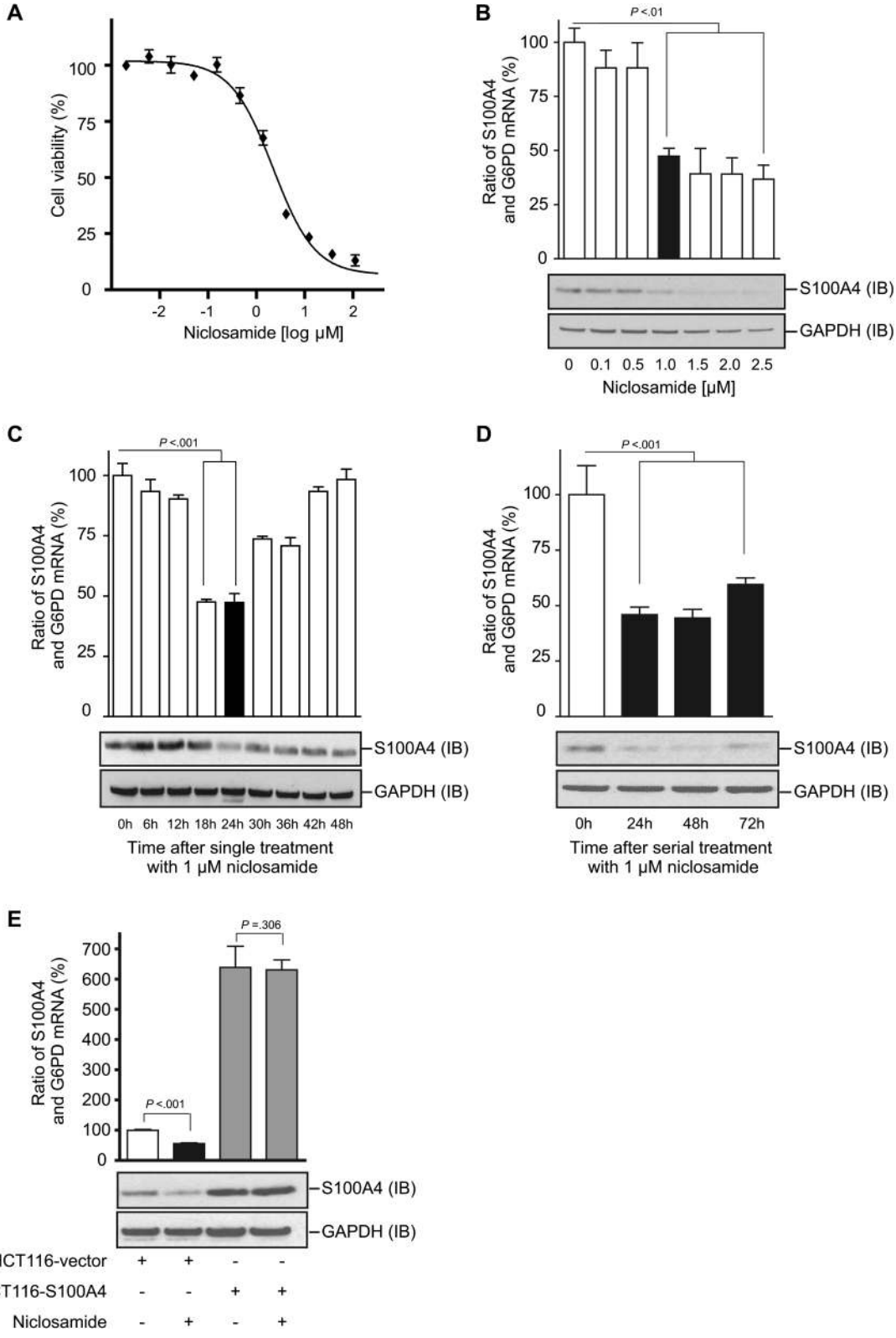

Figure 2. Effect of niclosamide on S100A4 mRNA and protein expression in human colon cancer cells. **A**) Assessment of cytotoxicity. HCT116 cells were treated with niclosamide (threefold dilutions starting with 3×10^2 μM concentration) for 24 hours. Cell viability was measured by Alamar blue assay and expressed as percent of untreated HCT116 cells (control). The means (**solid diamonds**) and **error bars** representing 95% confidence intervals from three independent experiments are presented. **B**) Effect of niclosamide on S100A4 expression. HCT116 cells were treated with increasing concentrations of niclosamide for 24 hours. S100A4 mRNA expression was determined by quantitative reverse transcription–polymerase chain reaction (qRT-PCR; normalized to the respective amount of G6PD mRNA for each condition) and

(continued)

control cells (schematic representation shown in Figure 1, B). In parallel, we assessed cell viability by Alamar blue assay to evaluate whether some of the inhibitory effects were caused by cytotoxicity. Of the 34 effective compounds, 11 compounds inhibited reporter gene expression at concentrations that were nontoxic or only slightly affected cell viability. To confirm the inhibitory capacity of the selected compounds and to more accurately establish the concentration–response curves, we performed a rescreening with these 11 compounds that were titrated using 20 twofold concentrations starting with the highest test concentration of 100 μM (Figure 1, B). Niclosamide showed inhibition of luciferase activity at 0.78 μM and higher concentrations and reduced cell viability at 3.1 μM and higher concentrations (Figure 1, C). Thus, the concentration–response assays confirmed niclosamide (2′,5-dichloro-4′-nitrosalicylanilide) as the strongest potential candidate for inhibition of reporter gene expression.

Effect of Niclosamide on S100A4 mRNA and Protein Expression

To determine an optimal working concentration of niclosamide, we tested the cytotoxicity of niclosamide on HCT116 cells. Treatment of HCT116 cells with increasing concentrations of niclosamide showed reduced cell viability in a concentration-dependent manner (EC_{50} = 2.2 μM, 95% confidence interval [CI] = 1.87 to 2.92 μM) (Figure 2, A). Next, we analyzed the effect of a range of concentrations of niclosamide (0.1–2.5 μM) on endogenous S100A4 expression in HCT116 cells and found that S100A4 mRNA and protein levels were reduced in a concentration-dependent manner (Figure 2, B). Niclosamide at greater than 0.5 μM concentrations reduced the endogenous S100A4 mRNA expression level to less than 50% of the solvent-treated control (1 μM niclosamide, mean = 47.4%, 95% CI = 39.3% to 55.4%, $P < .01$; 1.5 μM niclosamide, mean = 39.2%, 95% CI = 11.4% to 89.7%, $P < .01$; 2 μM niclosamide, mean = 39.1, 95% CI = 18.3% to 59.9%, $P < .01$; 2.5 μM niclosamide, mean = 36.7%, 95% CI = 18.6% to 54.8%, $P < .001$), analyzed by qRT-PCR. Similar effects were observed for S100A4 protein level analyzed by immunoblot assay (Figure 2, B). No change in S100A4 expression was detected with concentrations less than 1 μM niclosamide. With respect to the optimal concentration that showed minimum cytotoxicity and maximum inhibition of S100A4 expression, we used 1 μM niclosamide for further experiments.

We next analyzed the time dependency of niclosamide-mediated reduction of S100A4 expression. After a single dose of 1 μM niclosamide, the S100A4 mRNA expression level in HCT116 cells was reduced to less than 50% of the solvent-treated control level after 18–24 hours (1 μM niclosamide, mean level at 18 hours = 47.5%, 95% CI = 43.9% to 51.1%, $P < .001$; mean level at 24 hours = 47.4%, 95% CI = 39.4% to 55.4%, $P > .001$), but returned to the control level after 30–48 hours (Figure 2, C). Similar effects were noted for the S100A4 protein level (Figure 2, C). When HCT116 cells were treated daily with 1 μM niclosamide, we observed a steady reduction of S100A4 mRNA expression levels to approximately 50% of solvent-treated control cells (1 μM niclosamide, mean level at 24 hours = 46.0%, 95% CI = 38.7% to 53.3%, $P < .001$; mean level at 48 hours = 44.5%, 95% CI = 32.2% to 56.8%, $P < .001$; mean level at 72 hours = 59.5%, 95% CI = 50% to 69.2%, $P < .001$) (Figure 2, D). Reduction in S100A4 protein expression was noted at 24 hours and remained reduced after 72 hours (Figure 2, D).

Similar to HCT116 wild-type cells, treatment of stably transfected HCT116-vector cells with niclosamide reduced the S100A4 mRNA expression compared with solvent-treated control cells (control vs 1 μM niclosamide, mean = 100% vs 57.8%, mean difference = 42.2%, 95% CI = 31.9% to 52.1%, $P < .001$) (Figure 2, E). In stably transfected HCT116-S100A4 cells, the S100A4 mRNA level was sixfold higher than in HCT116-vector cells because of ectopic expression of the CMV promoter–driven S100A4 cDNA construct. Consequently, S100A4 protein expression was increased in HCT116-S100A4 cells. In contrast to HCT116-vector cells, treatment of HCT116–S100A4 with 1 μM niclosamide resulted in no reduction of S100A4 mRNA level compared with solvent-treated cells (control vs niclosamide, mean = 717.0% vs 612.3%, mean difference = 104.7%, 95% CI = 110.0% to 319.5%, $P = .306$), and similar results were noted for S100A4 protein levels.

Figure 2 (continued).

expressed as percent of solvent-treated HCT116 cells. The means and **error bars** representing 95% confidence intervals from three independent experiments are presented. *P* values were calculated using two-sided Student *t* test. **Black bar** indicates the chosen treatment conditions for further experiments. S100A4 protein levels were analyzed by immunoblot assay. GAPDH was used as the protein loading control. One representative blot of three independent experiments is presented. **C**) Time-dependent effect of niclosamide on S100A4 expression. HCT116 cells were treated with a single dose of 1 μM niclosamide for 24 hours, and S100A4 mRNA expression was analyzed by qRT-PCR (expressed as percent of solvent-treated HCT116 cells). The means and **error bars** representing 95% confidence intervals from three independent experiments are presented. *P* values were calculated using two-sided Student *t* test. **Black bar** indicates the chosen treatment conditions for further experiments. S100A4 protein levels were analyzed by immunoblot at the indicated time points. One representative blot of three independent experiments is presented. **D**) Effect of serial doses of niclosamide on S100A4 expression. HCT116 cells were treated daily with 1 μM niclosamide, and S100A4 mRNA expression was analyzed by qRT-PCR (expressed as percent of solvent-treated HCT116 cells). The means and **error bars** representing 95% confidence intervals from three independent experiments are presented. *P* values were calculated using two-sided one-way analysis of variance and Bonferroni post hoc multiple comparison test. **Black bars** indicate cells that were treated with 1μM niclosamide for 24 hours. S100A4 protein levels were analyzed by immunoblot at the indicated time points. One representative blot of three independent experiments is presented. **E**) Effect of niclosamide in HCT116-vector and HCT116–S100A4 cells. HCT116-vector (**white bar** represents solvent-treated control and **black bar** represents niclosamide treatment) and HCT116-S100A4 cells (represented by **gray bars**) were treated with 1 μM niclosamide for 24 hours, and S100A4 mRNA was analyzed by qRT-PCR (expressed as percent of solvent-treated HCT116-vector cells) The means and 95% confidence intervals (**error bars**) from three independent experiments are presented. S100A4 protein levels were analyzed by immunoblot. One representative blot of three independent experiments is presented. *P* values were calculated using two-sided Student *t* test. IB = immunoblot.

Effect of Niclosamide on Migration, Invasion, Proliferation, and Colony Formation of Cells Overexpressing S100A4

Cell Migration and Invasion. S100A4 is a main regulator of cell motility (25). Thus, we performed a Boyden chamber assay to analyze S100A4-induced cell migration in HCT116–S100A4 cells and assess whether niclosamide showed an effect on S100A4-induced cell migration. HCT116-vector cells treated with niclosamide showed inhibition of cell migration to less than 50% of solvent-treated control cells (control vs 1 μM niclosamide, mean = 100.0% vs 43.0%, mean difference = 57.0%, 95% CI = 40.3% to 73.7%, $P < .001$) (Figure 3, A). In contrast, HCT116–S100A4 cells treated with niclosamide for 24 hours showed no statistically significant inhibition of migration compared with solvent-treated cells (control vs 1 μM niclosamide, mean = 145.0% vs 117.0%, mean difference = 28%, 95% CI = 7.8% to 63.9%, $P = .118$).

Because S100A4 is known to stimulate cell invasion (11), we performed a Matrigel-covered Boyden chamber assay to determine whether niclosamide showed an effect on the invasion of HCT116-vector and HCT116–S100A4 cells. Treatment of HCT116-vector cells with niclosamide reduced cell invasion to 30% of solvent-treated control cells (control vs 1 μM niclosamide, mean = 100% vs 30.1%, mean difference = 69.9%, 95% CI = 10.9% to 128.9%, $P = .021$) (Figure 3, B). In contrast, niclosamide treatment had no effect on the invasion rate of HCT116–S100A4 cells compared with solvent-treated cells (control vs niclosamide, mean = 111.4% vs 122.5%, mean difference = 11.1%, 95% CI = 54.9% to 32.8%, $P = .617$).

We further analyzed the effect of niclosamide on directed migration in a wound healing assay. In the absence of niclosamide, HCT116-vector and HCT116–S100A4 cells completely closed the inserted wound after 4 days (Figure 3, C). Wound closure was impaired in niclosamide-treated HCT116-vector cells. In contrast, HCT116–S100A4 cells were able to migrate into the wound and close the gap despite the presence of niclosamide. In summary, treatment with niclosamide restricted cell motility and invasiveness. Ectopic overexpression of S100A4 was able to overcome niclosamide-mediated inhibition of cell motility, suggesting that the effect was specific to S100A4.

Cell Proliferation and Colony Formation. We measured anchorage-dependent cell proliferation in the presence or absence of niclosamide in HCT116-vector and HCT116–S100A4 cells. Treatment of both HCT116-vector and HCT116–S100A4 cells with niclosamide showed a reduced rate of cell proliferation that was independent of the expression level of S100A4 (Figure 3, D). Anchorage-independent growth was analyzed by colony formation assay. Solvent-treated HCT116-vector and HCT116–S100A4 cells were both able to form large colonies within 7 days (Figure 3, E). However, treatment with niclosamide clearly reduced the colony size of HCT116-vector and HCT116–S100A4 cells. Further, the number of HCT116-vector and HCT116–S100A4 cell colonies was severely reduced (HCT116-vector, control vs niclosamide, mean = 100% vs 6.8%, mean difference = 93.2%, 95% CI = 84.2 to 102.2%, $P < .001$; HCT116–S100A4, control vs niclosamide, mean = 105.8% vs 5.0%, mean difference = 100.8%, 95% CI = 89.5% to 111.9%, $P < .001$) (Figure 3, F). These results indicated that niclosamide-induced inhibition of cell proliferation and colony formation was independent of the level of endogenous or ectopic S100A4 expression.

Effect of Niclosamide on S100A4-Induced Cell Migration, Invasion, and Proliferation of Other Human Colon Cancer Cells

Next, we analyzed the effects of niclosamide on S100A4 expression in the colon cancer cell lines SW620, LS174T, SW480, and DLD-1. Niclosamide treatment reduced the S100A4 mRNA level in SW620, LS174T, and SW480 cells to less than 30% of the respective solvent-treated control (control vs 1 μM niclosamide, SW620, mean = 100.0% vs 31.2%, mean difference = 68.8%, 95% CI = 49.1% to 88.5%, $P < .001$; LS174T, mean = 65.5% vs 13.5%, mean difference = 52%, 95% CI = 38.3% to 65.6%, $P < .001$, SW480, mean = 41.0% vs 6.0%, mean difference = 35.0%, 95% CI = 27.1% to 42.9%, $P < .001$) (Figure 4, A). In DLD-1 cells, the S100A4 mRNA was barely detectable and remained unchanged under niclosamide treatment. Further, niclosamide reduced the S100A4 protein expression in SW620, LS174T, and SW480 cells, whereas no S100A4 protein was detected in solvent-treated and niclosamide-treated DLD-1 cells.

Niclosamide treatment for 24 hours reduced the cell migration rate of SW620, LS174T, and SW480 cells to less than 50% of the respective solvent-treated control (control vs niclosamide; SW620, mean = 100.0% vs 47.9%, mean difference = 52.1%, 95% CI = 25.4% to 78.9%, $P = .001$; LS174T, mean = 68.2% vs 26.8%, mean difference = 41.4%, 95% CI 16.3% to 66.3%, $P = .002$; SW480, mean = 21.7% vs 10.6% mean difference = 11.1%, 95% CI = 1.2% to 2.1%, $P = .030$). Solvent-treated DLD-1 cells presented the lowest migration rate after 24 hours, which was not further affected by niclosamide treatment (Figure 4, B). Similarly, cell invasion of SW620, LS174T, and SW480 cells was inhibited to less than 30% of the respective solvent-treated control (control vs niclosamide, SW620, mean = 100.0% vs 25.1%, mean difference = 74.9%, 95% CI = 48.4% to 101.4%, $P < .001$; LS174T, mean = 63.2% vs 23.6%, mean difference = 39.6%, 95% CI = 8.7% to 70.4%, $P = .013$; SW480, mean = 47.7% vs 12.8%, mean difference = 34.9%, 95% CI = 12.3% to 57.5%, $P = .003$) (Figure 4, C). The low invasion rate of solvent-treated DLD-1 cells after 24 hours was not affected by niclosamide treatment ($P = .641$). Directed migration of SW620, LS174T, SW480, and DLD-1 cells, as measured in the wound healing assay, was impaired upon niclosamide treatment compared with the respective solvent-treated control (Figure 4, D). Consistent with their lower migration rate, solvent-treated DLD-1 cells did not close the wound until day 4.

Anchorage-dependent cell proliferation of all four cell lines was inhibited under niclosamide treatment (Figure 4, E). Moreover, anchorage-independent growth was impaired when SW620, LS174T, SW480, and DLD-1 cells were treated with niclosamide, resulting in clearly smaller cell colonies (Figure 4, F). Niclosamide treatment reduced the number of colonies to less than 50% in all four colon cancer cells lines (control vs niclosamide, SW620, mean = 100.0% vs 3.6%, mean difference = 96.4%, 95% CI = 78.0% to 114.8%, $P < .001$; LS174T, mean = 90.6% vs 15.9%, mean difference = 74.7%, 95% CI = 58.3% to 91.0%, $P < .001$; SW480, mean = 68.1% vs 4.3%, mean difference = 63.8%, 95% CI = 52.2% to 75.4%, $P < .001$; DLD-1, mean = 82.6% vs 10.1%, mean

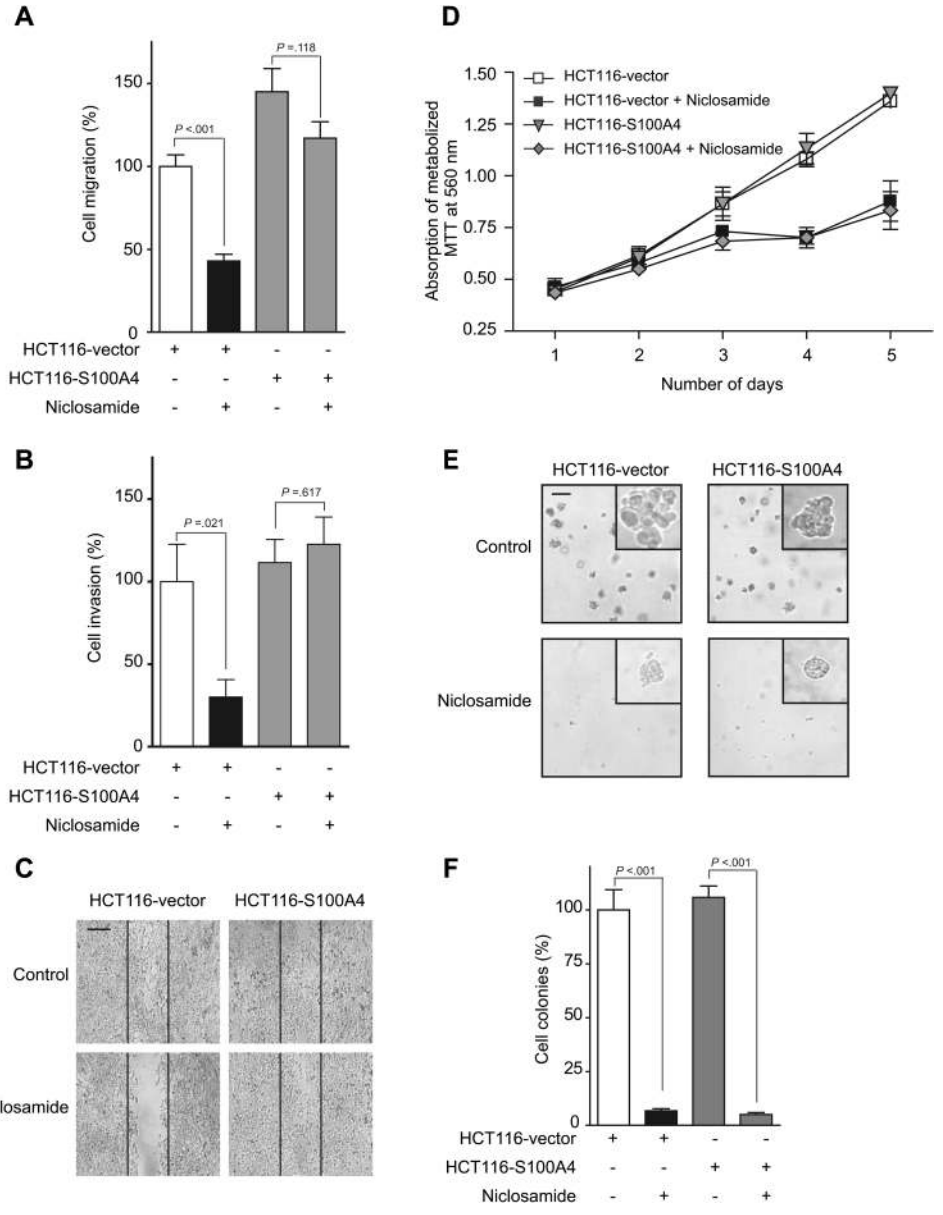

Figure 3. Effect of niclosamide on cell migration and proliferation. **A**) Cell migration of HCT116-vector (**white bar** represents solvent-treated control and **black bar** represents niclosamide treatment) and HCT116–S100A4 cells (represented by **gray bars**). Cells were treated with 1 μM niclosamide for 24 hours. Cell migration was analyzed using Boyden chamber assay and expressed as percentage of solvent-treated HCT116-vector cells. The means and 95% confidence intervals (**error bars**) from three independent experiments are presented. *P* values were calculated using two-sided Student *t* test. **B**) Cell invasion of HCT116-vector and HCT116–S100A4 cells treated with niclosamide as in (**A**). Cell invasion was analyzed using Boyden chamber assay and expressed as percent of solvent-treated HCT116-vector cells. The means and 95% confidence intervals from six independent experiments are presented. *P* values were calculated using two-sided Student *t* test. **C**) Directed migration of HCT116-vector and HCT116–S100A4 cells treated with niclosamide analyzed by wound healing assay. Wounds of 300 μM width were set in a 60% confluent monolayer of HCT116-vector or HCT116–S100A4 cells on day 1. Cells were treated daily with 1 μM niclosamide for 4 days. The **vertical black lines** indicate the margins of wound on day 1. Representative micrographs from day 4 are shown. Magnification = ×10. Scale bar = 200 μM. **D**) Anchorage-dependent cell proliferation of HCT116-vector and HCT116 –S100A4 cells treated daily with 1 μM niclosamide. Cell proliferation was determined by 3-(4,5-dimethyl-2-thiazol)-2,5-diphenyl-2H-tetrazolium bromide (MTT) assay. **E**) Anchorage-independent cell growth of HCT116-vector and HCT116–S100A4 cells treated with niclosamide. Cells were plated as single cells in 0.33% (wt/vol) agarose and treatment (solvent or 1 μM niclosamide) containing medium. After 7 days, colonies were visualized by light microscopy. Magnification = ×10 (overview) and ×40 (inset showing a single colony). Scale bar = 200 μM. **F**) Quantification of colonies. Number of colonies (consisting of more than four cells) was counted and normalized to solvent-treated HCT116-vector cells. The means and 95% confidence intervals from two independent experiments are presented. *P* values were calculated using two-sided Student *t* test.

difference = 72.5%, 95% CI = 52.5% to 92.4%, $P < .001$) (Figure 4, G). In summary, in colon cancer cells with increased S100A4 expression levels, niclosamide inhibited cell migration and invasion. Moreover, niclosamide inhibited cell proliferation in colon cancer cells independent on the endogenous S100A4 expression level.

Effect of Niclosamide Derivatives on S100A4 Expression and Cell Migration

We analyzed the effect of structural changes in the niclosamide molecule on its ability to inhibit S100A4 expression. To compare the efficiency of niclosamide and its derivatives (Figure 5, A) to inhibit S100A4 expression, HCT116 cells were treated with all compounds at the same treatment conditions defined for niclosamide and analyzed for S100A4 mRNA and protein levels (Figure 5, B). In contrast to the observed effects of niclosamide, no reduction of S100A4 mRNA and protein levels were detected with any of the six niclosamide derivatives. Analysis of cell migration showed reduced migration only after niclosamide treatment, but not after treatment with any of the six derivative compounds (Figure 5, C). In summary, none of the niclosamide derivatives was more effective than niclosamide in inhibiting S100A4 expression and S100A4-induced cell motility. These results indicate that changes in the structure of niclosamide result in loss of its efficiency toward inhibition of S100A4 expression.

Effect of Niclosamide on the WNT/CTNNB1 Pathway

Constitutively Active WNT Signaling Pathway. It was previously shown that S100A4 is a transcriptional target gene of the WNT/CTNNB1 pathway and that HCT116 cells are heterozygous for mutated CTNNB1, resulting in constitutively active WNT signaling pathway and S100A4 expression (4,20). Using the LEF/

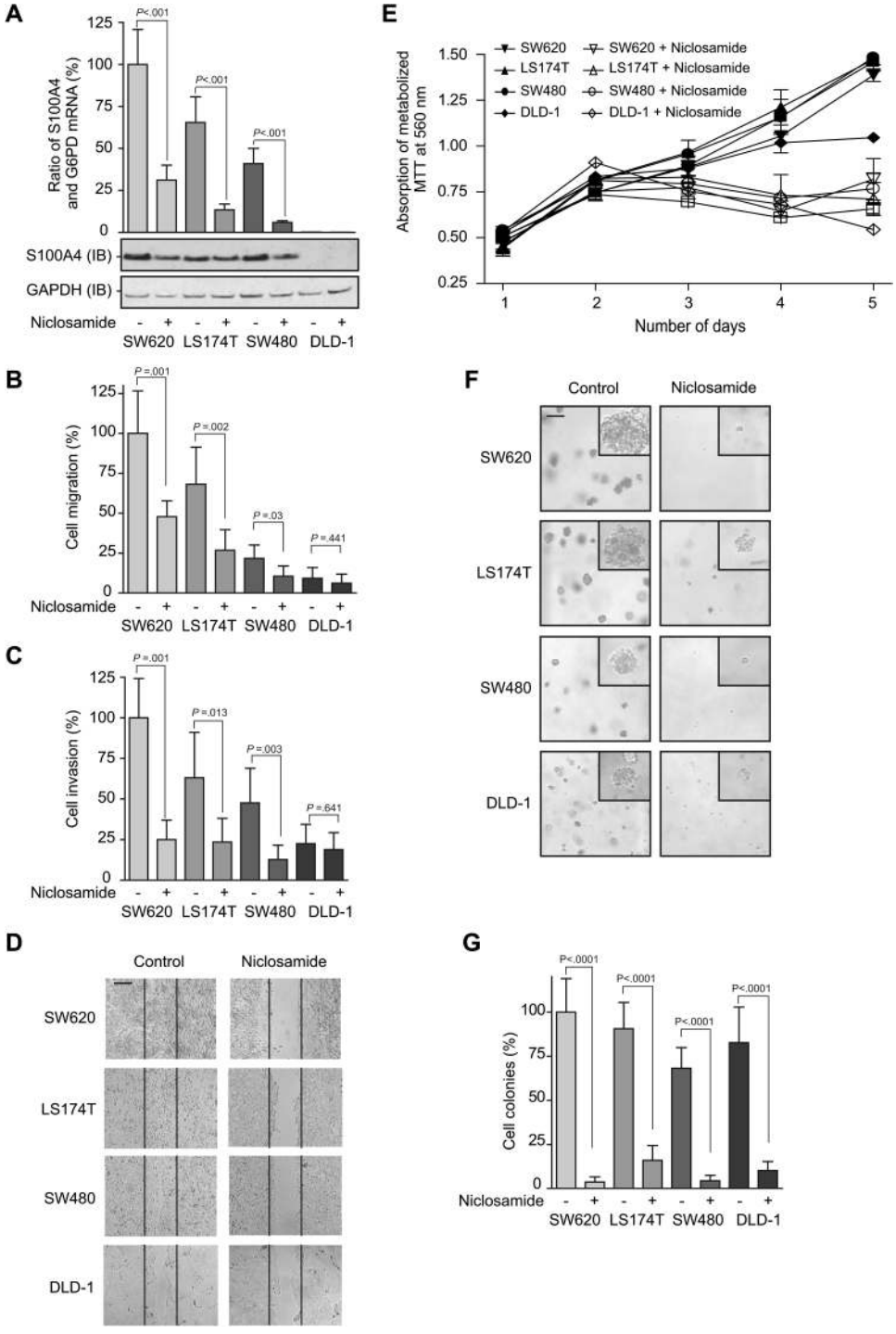

Figure 4. Effect of niclosamide on multiple colon cancer cell lines. SW620, LS174T, SW480, and DLD-1 cell lines were used (each cell line is represented by different shade of **gray**). **A**) S100A4 expression of niclosamide-treated cells. Cells were treated with 1 μM niclosamide for 24 hours. S100A4 mRNA expression was determined by quantitative reverse transcription–polymerase chain reaction (normalized to the respective amount of G6PD mRNA for each condition and cell line) and expressed as percent of solvent-treated SW620 cells. The means and 95% confidence intervals (**error bars**) from three independent experiments are presented. *P* values were calculated using two-sided Student *t* test. S100A4 protein levels were analyzed by immunoblot assay. GAPDH was used as the protein loading control. One representative blot of two independent experiments is shown. **B**) Cell migration of niclosamide-treated cells. Cells were treated as in panel (**A**). Cell migration was determined using Boyden chamber assay and expressed as percent of solvent-treated SW620 cells. The means and 95% confidence intervals from three independent experiments are presented. *P* values were calculated using two-sided Student *t* test. **C**) Cell invasion of niclosamide-treated cells. Cells were treated as in panel (**A**). Cell invasion was analyzed using Boyden chamber assay and expressed as percent of solvent-treated SW620 cells. The means and 95% confidence intervals from six independent experiments are presented. *P* values were calculated using two-sided Student *t* test. **D**) Directed migration of niclosamide-treated cells. Wounds of 300 μM width were set in a 60% confluent monolayer of cells on day 1. Cells were treated daily with 1 μM niclosamide for 4 days. Representative microphotographs from day 4 are shown. The **vertical black lines** indicate the margins of wound on day 1. Magnification = ×10. Scale bar = 200 μM. **E**) Anchorage-dependent cell proliferation of niclosamide-treated cells. Cells were treated daily with 1 μM niclosamide. Cell proliferation was determined using 3-(4,5-dimethyl-2-thiazol)-2,5-diphenyl-2H-tetrazolium bromide (MTT) assay. **F**) Anchorage-independent cell growth of niclosamide-treated cells. Cells were plated as single cells in 0.33% (wt/vol) agarose and treatment (solvent or 1 μM niclosamide) containing medium. After 7 days, colonies were visualized by light microscopy. Magnification = ×10 (overview) and × 40 (inset showing a single colony). Scale bar = 200 μM. **G**) Quantification of colonies. Number of colonies (of more than four cells) was counted and normalized to solvent-treated SW620 cells. The means and 95% confidence intervals from two independent experiments are presented. *P* values were calculated using two-sided Student *t* test. IB = immunoblot.

TCF transcription factor reporter (TOP/FOPflash) assay, we analyzed WNT/CTNNB1 pathway activity in niclosamide-treated HCT116 cells, which carry a wild-type and mutated allele of CTNNB1. We further used the HCT116-derivative cells, HAB-68^{mut} and HAB-92^{wt}, which carry only the mutated or the wild-type allele of CTNNB1, respectively. Treatment with 1 μM niclosamide showed reduced WNT pathway activity in HCT116, HAB-68^{mut}, and HAB-92^{wt} cells (control vs niclosamide expressed as fold difference in activity, HCT116, mean = 1.00 vs 0.39, mean difference = 0.61, 95% CI = 0.41 to 0.81, $P < .001$; HAB-68^{mut}, mean = 1.39 vs 0.50, mean difference = 0.90, 95% CI = 0.64 to 1.16, $P < .001$; HAB-92^{wt}, mean = 0.36 vs 0.21, mean difference = 0.15, 95% CI = 0.05 to 0.25, $P = .007$). Treatment with niclosamide also showed reduced S100A4 mRNA and protein expression (control vs niclosamide expressed as fold difference in expression level, HCT116, mean = 1.00 vs 0.46, mean difference = 0.54, 95% CI = 0.43 to 0.65, $P < .001$; HAB-68^{mut},

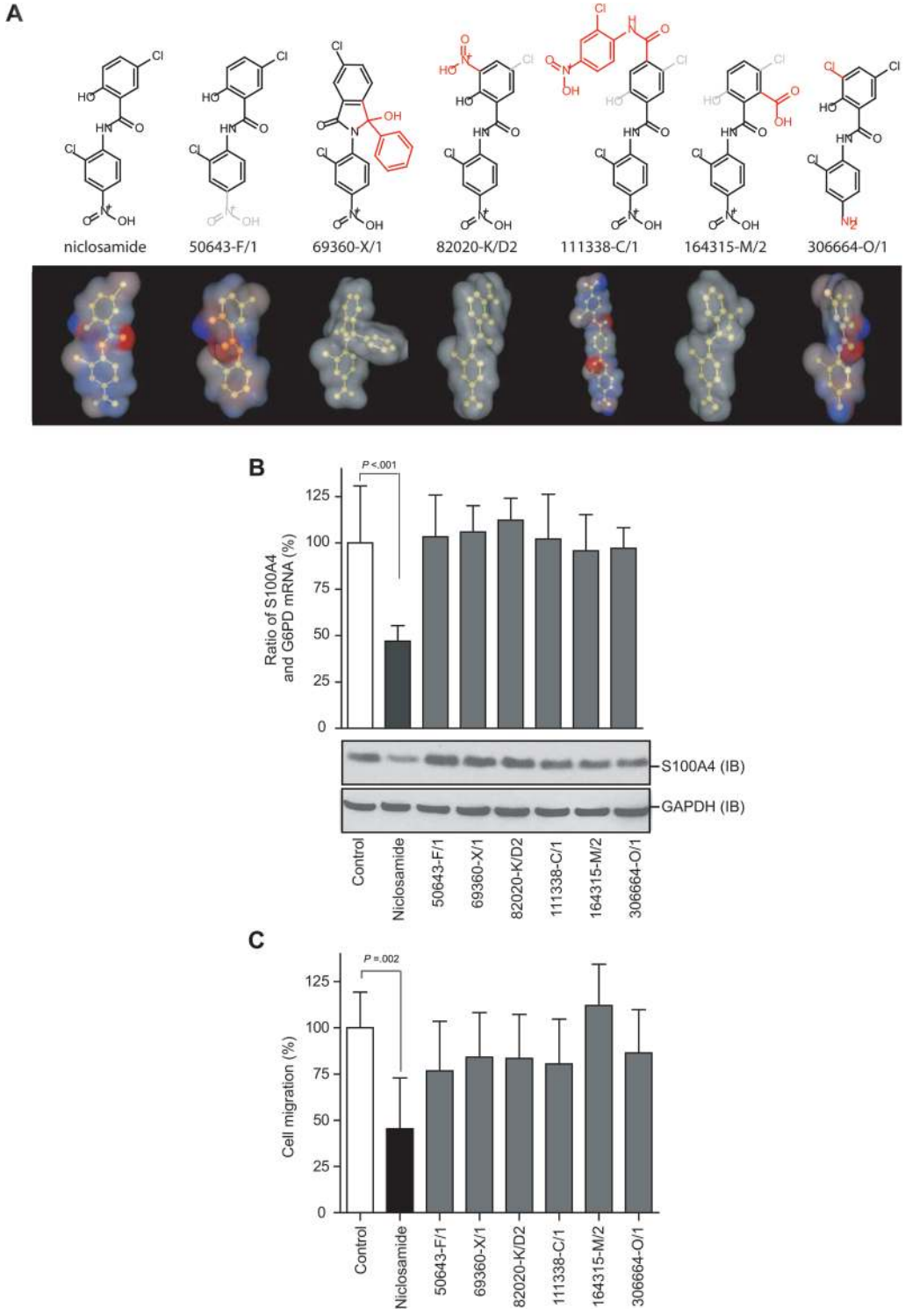

Figure 5. Effect of niclosamide and its derivatives on S100A4 expression and S100A4-induced cell migration. **A**) Chemical structure of niclosamide and its derivatives. Top panel: Two-dimensional illustrations showing the added chemical groups in **red** and the lost chemical groups in **gray**. Bottom panel: Three-dimensional illustrations showing the negative and positive charges in **red** and **blue**, respectively, and **gray clouds** representing the van der Waals surface. **B**) Effect of niclosamide and its derivatives on S100A4 expression. HCT116 cells were treated with 1 μM niclosamide (indicated by **black bar**) or its derivatives (indicated by **gray bars**) for 24 hours. S100A4 mRNA expression was determined by quantitative reverse transcription–polymerase chain reaction (normalized to the respective amount of G6PD mRNA for each condition) and expressed as percent of solvent-treated HCT116 cells. The means and 95% confidence intervals (**error bars**) from three independent experiments are presented. *P* values were calculated using two-sided one-way analysis of variance (ANOVA) and Bonferroni post hoc multiple comparison tests. S100A4 protein levels were analyzed by immunoblot assay. GAPDH was used as the protein loading control. One representative blot of four independent experiments is shown. **C**) Effect of niclosamide or its derivatives on cell migration. HCT116 cells were treated as in panel (**B**). Cell migration was determined using Boyden chamber assay and expressed as percent of solvent-treated HCT116 cells. The means and 95% confidence intervals from two independent experiments are presented. *P* values were calculated using two-sided one-way ANOVA and Bonferroni post hoc multiple comparison tests. IB = immunoblot.

mean = 1.17 vs 0.62, mean difference = 0.55, 95% CI = 0.41 to 0.69, $P < .001$; HAB-92^{wt}, mean = 0.03 vs 0.01, mean difference = 0.02, 95% CI = −0.001 to 0.047, $P = .060$) (Figure 6, B). Consistently, migration rates of HCT116 and HAB-68^{mut} cells were reduced to the level of HAB-92^{wt} cells upon niclosamide treatment (control vs niclosamide expressed as fold difference in migration rate, HCT116, mean = 1.00 vs 0.45, mean difference = 0.54, 95% CI = 0.22 to 0.87, $P = .002$; HAB-68^{mut}, mean = 1.30 vs 0.39, mean difference = 0.91, 95% CI = 0.62 to 1.20, $P < .001$; HAB-92^{wt}, mean = 0.36 vs 0.32, mean difference = 0.04, 95% CI = −0.08 to 0.16, $P = .497$) (Figure 6, C). In summary, niclosamide inhibits WNT signaling–dependent target gene transcription, such as the transcription of S100A4, despite a constitutively active WNT/CTNNB1 pathway.

Mode of Action on the CTNNB1/TCF Transcription Complex. Active WNT signaling is dependent on nuclear CTNNB1 activity. Accordingly, we analyzed the amount of nuclear CTNNB1 under increasing concentrations of niclosamide. Treatment of HCT116

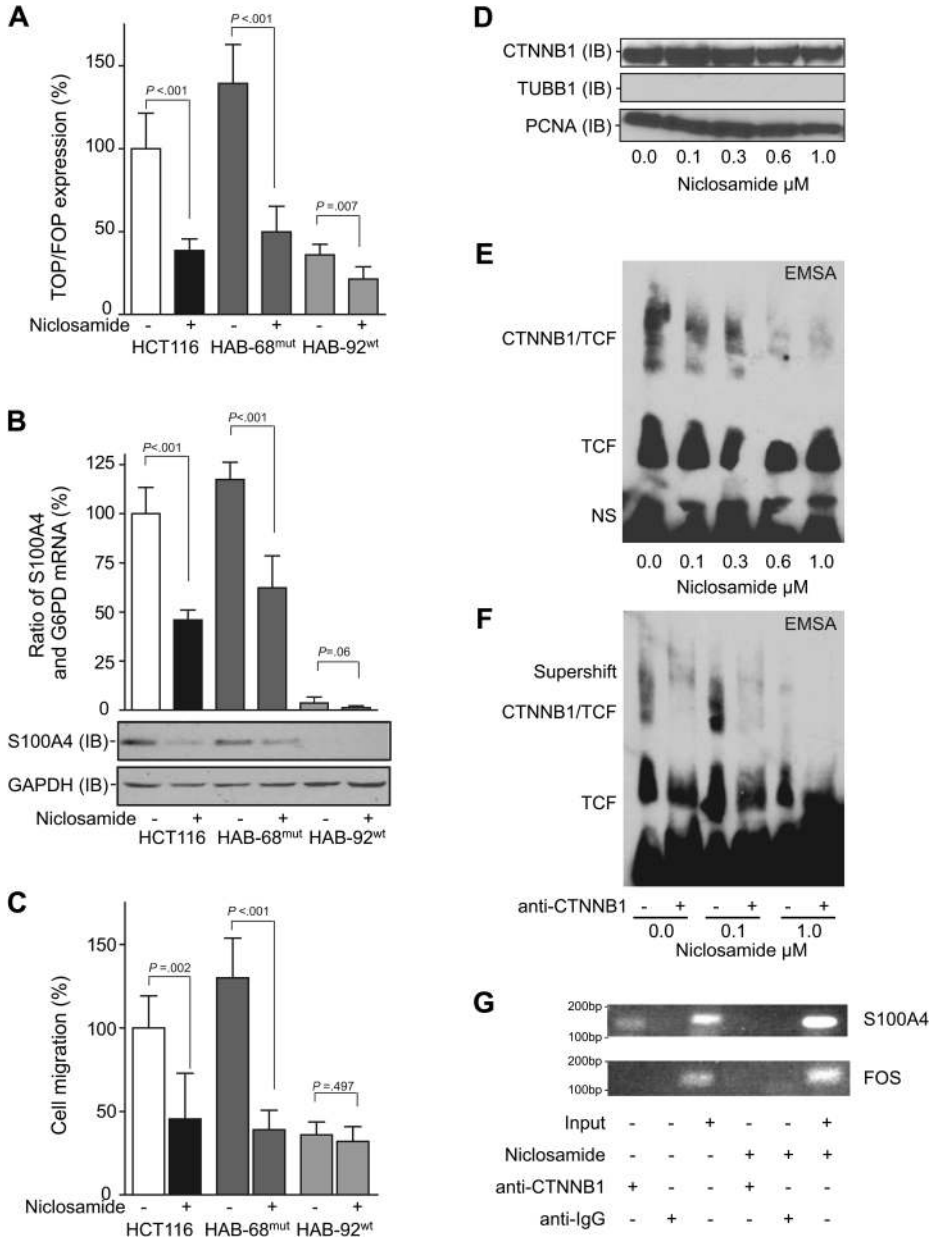

Figure 6. Effect of niclosamide on constitutively active WNT/CTNNB1 pathway signaling. HCT116 cells (heterozygous for gain-of-function mutated CTNNB1, represented by **white bar** for solvent-treated control and **black bar** for niclosamide treatment); HAB-68^{mut} cells (deletion mutant of HCT116, expressing only gain-of-function mutated CTNNB1; represented by dark **gray bars**); and HAB-92^{wt} cells (deletion mutant of HCT116, expressing only wild-type CTNNB1; represented by **light gray bars**) were used. **A**) Effect of niclosamide on LEF/TCF reporter gene expression in HCT116, HAB-68^{mut}, and HAB-92^{wt} cells. Cells were treated with 1 μM niclosamide for 24 hours. Reporter gene expression was determined by measuring the luciferase activity. For each condition and cell line, TOPflash expression was normalized to FOPflash expression. The means and 95% confidence intervals (**error bars**) from three independent experiments are presented. *P* values were calculated using two-sided Student *t* test. **B**) Effect of niclosamide on S100A4 expression in HCT116, HAB-68^{mut}, and HAB-92^{wt} cells. Cells were treated as in panel (**A**). S100A4 mRNA expression was determined by quantitative reverse transcription–polymerase chain reaction (normalized to the respective amount of G6PD mRNA for each condition and cell line) and expressed as percent of solvent-treated HCT116 cells. The means and 95% confidence intervals from three independent experiments are presented. *P* values were calculated using two-sided Student *t* test. S100A4 protein levels were analyzed by immunoblot assay. GAPDH was used as the protein loading control. One representative blot of two independent experiments is shown. **C**) Effect of niclosamide on migration of HCT116, HAB-68^{mut}, and HAB-92^{wt} cells. Cells were treated as in panel (**A**), and cell migration was analyzed using Boyden chamber assay. Cell migration was expressed as percent of solvent-treated HCT116 cells. The means and 95% confidence intervals from three independent experiments are presented. *P* values were calculated using two-sided Student *t* test. **D**) Effect of niclosamide on the nuclear localization of CTNNB1. HCT116 cells were treated with the indicated concentrations of niclosamide for 18 hours, and the amount of nuclear CTNNB1 protein was analyzed by immunoblot of nuclear extracts. Cytoplasmic TUBB1 was used as control for contamination of nuclear extracts with cytoplasmic proteins. Proliferating cell nuclear antigen was used as the protein loading control. One representative blot of three independent experiments is shown. **E**) Effect of niclosamide on the CTNNB1/TCF complex. HCT116 cells were treated as in panel (**D**). The presence of the CTNNB1/TCF complex on the S100A4 promoter site was analyzed by electrophoretic mobility shift assay (EMSA). One representative EMSA of two is shown. **F**) HCT116 cells were treated with indicated concentrations of niclosamide for 18 hours. The presence of CTNNB1 in the CTNNB1/TCF complex at the S100A4 promoter was analyzed by supershift via addition of a monoclonal mouse anti-human CTNNB1 antibody (anti-CTNNB1). **G**) Effect of niclosamide on the presence of CTNNB1 at the S100A4 promoter. HCT116 cells were treated with 1 μM niclosamide for 18 hours and processed for chromatin immunoprecipitation assay. Soluble chromatin was immunoprecipitated with a monoclonal anti-CTNNB1 antibody or a nonspecific control IgG antibody. The input verified the integrity of the polymerase chain reaction. The FOS promoter sequence to which CTNNB1 does not bind was used as control. Data represent two independent experiments. IB = immunoblot; FOS = FBJ murine osteosarcoma viral oncogene homolog; IgG = immunoglobulin; NS = nonspecific free oligonucleotide–protein complex.

cells with increasing concentrations of niclosamide for 18 hours did not change the protein level of nuclear CTNNB1 (Figure 6, D). However, we did observe a reduction in WNT/CTNNB1 signaling and in S100A4 gene expression (Figure 6, A and B). Therefore, we hypothesized that niclosamide may act within the nucleus to inhibit the formation of the CTNNB1/TCF transcription activating complex. This hypothesis was tested by EMSA, using biotinylated oligonucleotides encompassing the TCF-binding site of the S100A4 promoter. Oligonucleotide shifts caused by binding with TCF and CTNNB1/TCF complex were detected in the absence of niclosamide (Figure 6, E), which is consistent with previous findings (4). Treatment of HCT116 cells to increasing concentrations of niclosamide interrupted the CTNNB1/TCF/oligonucleotide complex in a concentration-dependent manner.

The presence of CTNNB1 within the complex was verified by the formation of a supershifted complex with monoclonal mouse anti-human CTNNB1 antibody. In nuclear extracts from solvent-treated HCT116 cells, the supershifted complex was detected (Figure 6, F). However, no supershifted complex was detected in nuclear extracts from 1 μM niclosamide-treated cells. Consistent with these results, the ChIP assay showed that no S100A4 promoter sequence could be PCR amplified after

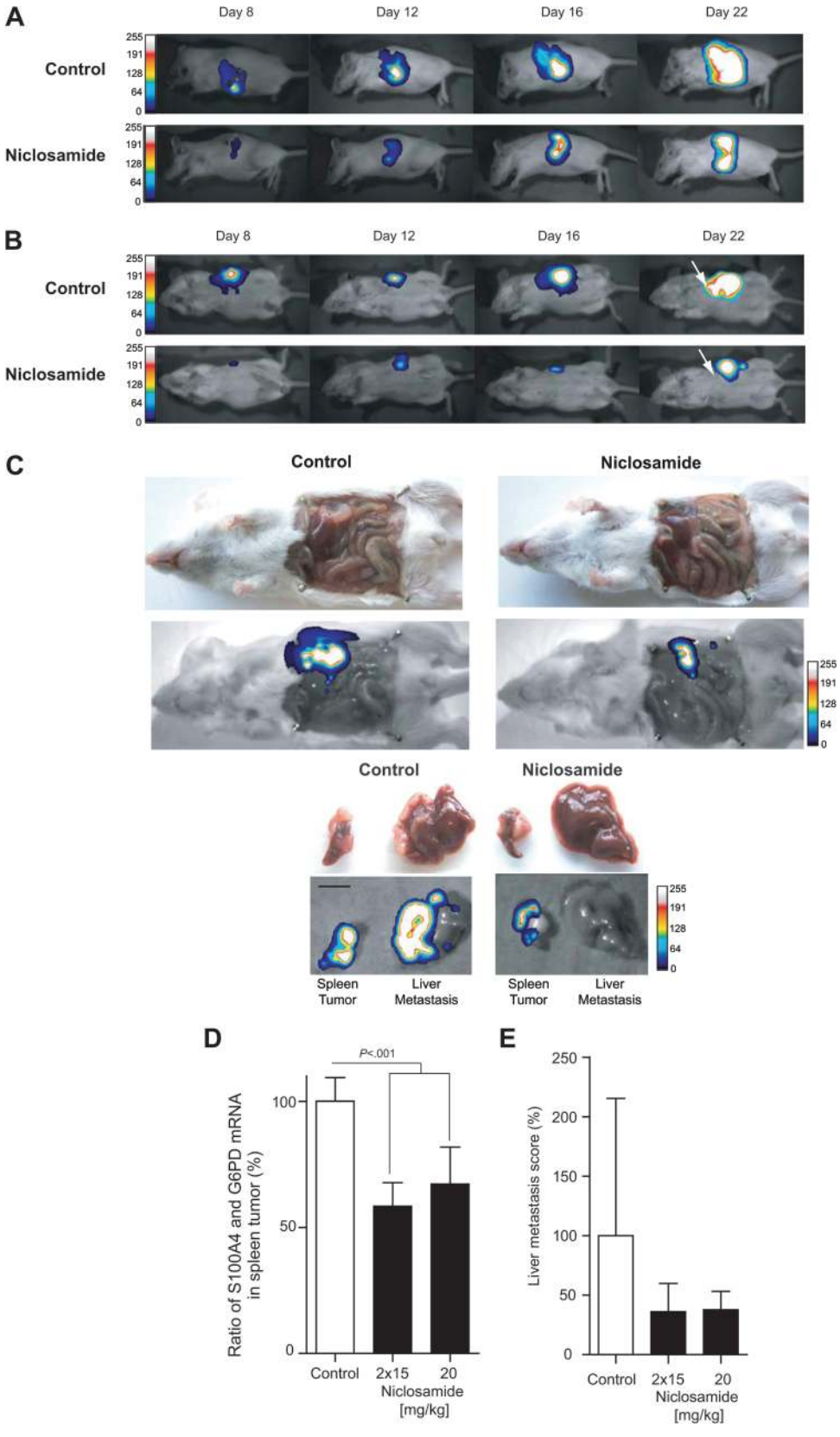

Figure 7. Effect of niclosamide on metastasis in a mouse xenograft model. In vivo luminescence imaging of metastasis formation in the liver. HCT116-CMVp-LUC cells stably expressing firefly luciferase (LUC) were intrasplenically transplanted into nonobese diabetic–severe combined immunodeficiency mice. Mice (n = 4 per group) were treated daily with intraperitoneal injections of solvent or 20 mg/kg niclosamide. For luminescence imaging, mice were anesthetized on the indicated days and given intraperitoneal injections of D-luciferin. Signal intensity of grayscale images (256 scale) were color coded (order of low to high signal intensity: **blue**, **green**, **yellow**, **red**, and **white**) and overlayed with bright field picture. **A**) Lateral imaging. **B**) Ventral imaging. The **arrows** indicate the location of the liver edge. **C**) In situ imaging of mice and isolated organs on day 24. Exposure time was 20 seconds per picture for panels (**A**) and (**B**), and 1 second per picture for panel (**C**). **D**) HCT116-CMVp-LUC cells were intrasplenically transplanted in mice (n = 9 per group), and mice were treated daily with solvent or 20 mg/kg niclosamide or twice-daily 15 mg/kg niclosamide for 24 days. On day 24, S100A4 mRNA expression was analyzed in the spleen tumors by quantitative reverse transcription–polymerase chain reaction and expressed as percentage of control mice. The means and 95% confidence intervals (**error bars**) of nine experiments are presented. *P* values were calculated using two-sided one-way analysis of variance and Bonferroni post hoc multiple comparison tests. **E**) Mice (n = 9 per group) were treated as in panel (**D**) and liver metastases were scored for number and size. The means and 95% confidence intervals are presented. In both (**D**) and (**E**), **white bar** represents solvent-treated control and **black bars** represent niclosamide treatment.

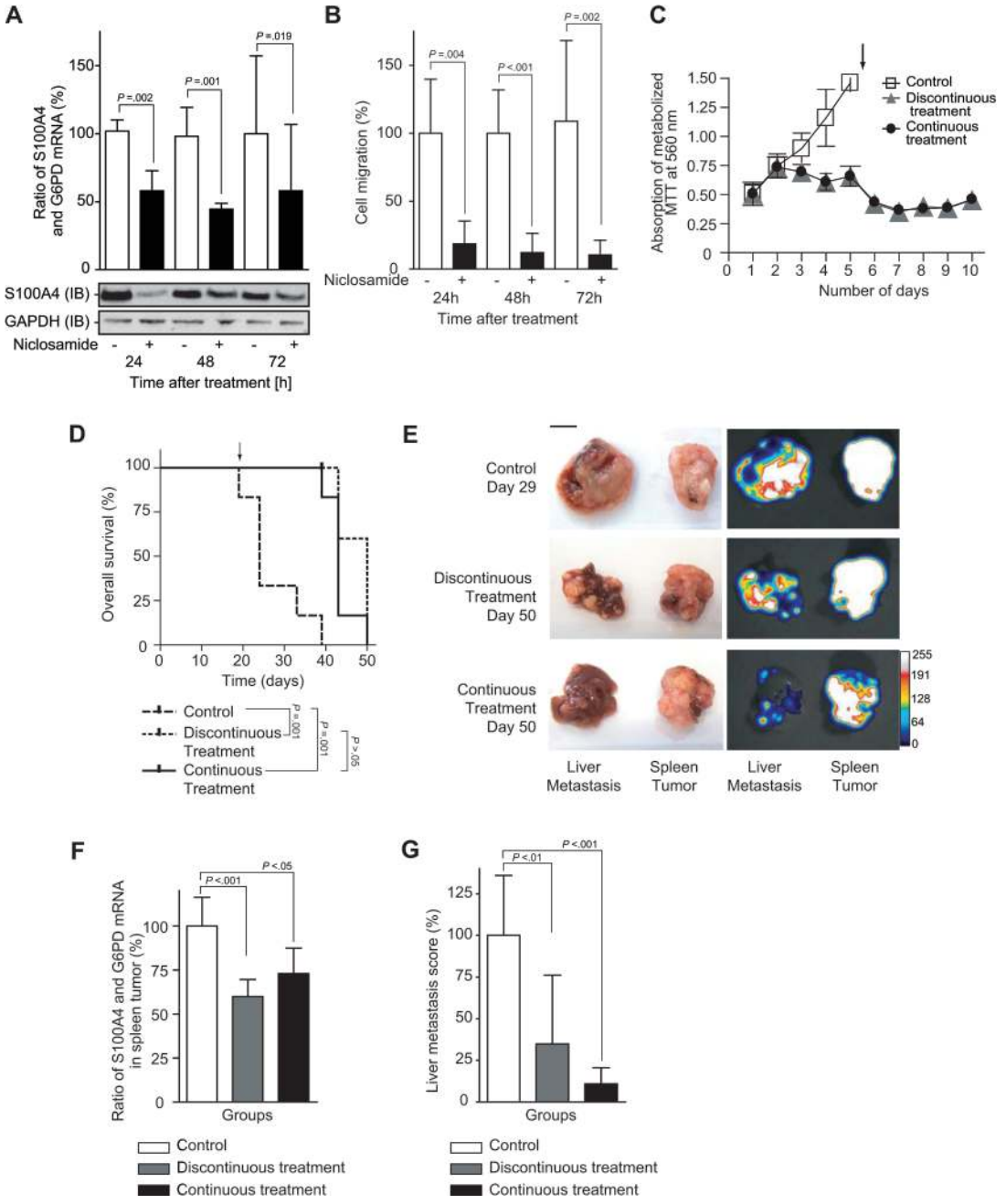

Figure 8. Long-term effects of niclosamide treatment in vitro and in vivo. **A**) S100A4 expression in vitro after discontinuation of niclosamide treatment. HCT116 cells were treated daily with 1 μM niclosamide for three consecutive days, medium was removed on day 4, and S100A4 expression was analyzed 24, 48, and 72 hours after niclosamide removal. S100A4 mRNA expression was determined by quantitative reverse transcription–polymerase chain reaction (qRT-PCR) (normalized to the respective amount of G6PD mRNA) and expressed as percent of solvent-treated HCT116 cells. The means and 95% confidence intervals (**error bars**) from three independent experiments are presented. *P* values were calculated using two-sided Student *t* test. S100A4 protein levels were analyzed by immunoblot assay. GAPDH was used as the protein loading control. One representative blot of two independent experiments is shown. **B**) Cell migration after discontinuation of niclosamide treatment. HCT116 cells were treated as in panel (**A**). Cell migration was analyzed using Boyden chamber assay and expressed as percentage of solvent-treated HCT116 cells. The means and 95% confidence intervals from three independent experiments are presented. *P* values were calculated using two-sided Student *t* test. In (**A**) and (**B**), **white bars** represent solvent-treated control and **black bars** represent niclosamide treatment. **C**) Anchorage-dependent cell proliferation after discontinuation of niclosamide treatment. HCT116 cells were treated with 1 μM niclosamide or solvent daily, or niclosamide for the first 5 days and solvent from day 5 on (**arrow** indicates discontinuation of treatment). Cell proliferation was determined using 3-(4,5-dimethyl-2-thiazol)-2,5-diphenyl-2H-tetrazolium bromide (MTT) assay. **D**) Overall survival of mice treated continuously and discontinuously with niclosamide. HCT116-CMVp-LUC cells were intrasplenically injected into nonobese diabetic–severe combined immunodeficiency mice (n = 6 per group) and treated intraperitoneally daily with either solvent or 20 mg/kg niclosamide or for the first 24 days with 20 mg/kg niclosamide followed by solvent (**arrow** indicates when the treatment was stopped). *P* values were calculated using two-sided log-rank test. **E**) Luminescence signal from liver metastases and spleen tumors. Mice (n = 6 per group) were treated as in panel (**D**), and intraperitoneally injected with D-luciferin 10 minutes before liver and spleen were removed and

(continued)

CTNNB1 immunoprecipitation from niclosamide-treated cell extracts, but PCR product was detected from solvent-treated cell extracts (Figure 6, G). The latter had been observed previously by Stein et al. (4). No PCR product could be detected when control IgG was used for precipitation or when a FOS promoter sequence was PCR amplified. In summary, the results indicated that niclosamide treatment inhibited the formation of CTNNB1/TCF complex and thereby inhibited transcription of WNT/CTNNB1 target gene S100A4.

Effect of Niclosamide on Metastasis Formation In Vivo

We next monitored the effect of niclosamide on metastasis formation over time in a mouse xenograft model by noninvasive in vivo luminescence imaging. Mice (n = 8) were intrasplenically injected with HCT116-CMVp-LUC cells, which stably expressed firefly luciferase, and were treated with daily doses of solvent as control (n = 4 mice) or 20 mg/kg niclosamide (n = 4 mice). On day 8 after transplantation, a visible spleen tumor signal in solvent- and niclosamide-treated mice was detected laterally, and the signal intensity as well as the signal area increased on day 12 and 16. The signal intensity reached its maximum on day 22 after transplantation (Figure 7, A). Ventral imaging of solvent- and niclosamide-treated mice also presented the lateral spleen tumor signal. However, in control mice, an additional signal from the edge of the liver was detected on day 8, which continued to increase until day 22. Such liver signals were absent in niclosamide-treated mice (Figure 7, B). In situ imaging of the liver and spleen as well as imaging of the removed spleen and liver (Figure 7, C) further confirmed that in control mice liver metastasis formation had occurred, but not in niclosamide-treated mice.

We next analyzed the S100A4 mRNA level by qRT-PCR in the spleen tumor of xenografted mice (n = 27) on day 24. Mice were treated either with daily doses of solvent (n = 9 mice) or 20 mg/kg niclosamide (n = 9 mice) or two doses of 15 mg/kg niclosamide twice daily (n = 9 mice) for 24 days. S100A4 mRNA levels were reduced in niclosamide-treated mice compared with solvent-treated control mice (control vs treated with 2 × 15 mg/kg niclosamide, mean = 100.0% vs 58.4%, mean difference = 41.6 %, 95% CI = 21.6% to 61.8%, $P < .001$; control vs treated with 1 × 20 mg/kg, mean = 100.0% vs 67.2%, mean difference = 32.8%, 95% CI = 14.1% to 51.7%, $P < .001$) indicating that niclosamide inhibited S100A4 expression in vivo (Figure 7, D). Moreover, liver metastasis score (n = 9 mice per group) was reduced in niclosamide-treated mice compared with solvent-treated mice (control, mean = 100.0%, 95% CI = −15.4% to 215.4%; treated with 2 × 15 mg/kg, mean = 36.1%, 95% CI = 12.4% to 59.8%; treated with 1 × 20 mg/kg, mean = 37.9%, 95% CI = 22.6% to 53.1%) (Figure 7, E). In summary, the results showed that niclosamide treatment inhibited S100A4-induced metastasis formation in vivo.

Long-term Effect of Niclosamide Treatment In Vitro and In Vivo

We next investigated the effect of discontinuation of niclosamide treatment on S100A4-mediated metastasis formation. We first treated HCT116 cells daily with 1 μM niclosamide for three consecutive days. On day 4, niclosamide was removed and S100A4 expression was assayed by qRT-PCR and immunoblot. As shown earlier in Figure 2, D, daily treatment of HCT116 cells with 1 μM niclosamide inhibited S100A4 mRNA and protein expression for three consecutive days. Interestingly, the S100A4 mRNA level remained reduced in HCT116 cells to approximately 50% of the respective solvent-treated control at 24, 48, and 72 hours after discontinuation of niclosamide treatment (control vs niclosamide, 24 hours after treatment, mean = 101.9% vs 58.0%, mean difference = 43.9%, 95% CI = 31.0% to 56.8%, $P = .001$; 48 hours after treatment, mean = 98.1% vs 44.4%, mean difference = 53.7%, 95% CI = 33.2% to 74.1%, $P = .001$; 72 hours after treatment, mean = 100.0% vs 57.9%, mean difference = 42.1%, 95% CI = 16.6% to 67.6%, $P = .019$) (Figure 8, A). Furthermore, the S100A4 protein level remained reduced for 3 days after discontinuation of the niclosamide treatment. Cell migration of HCT116, analyzed using the Boyden chamber assay, continued to show a reduced level of less than 20% of the respective solvent-treated control for up to 3 days after discontinuation of niclosamide treatment (control vs niclosamide, 24 hours after treatment, mean = 100.0% vs 18.7%, mean difference = 81.3%, 95% CI = 40.7% to 122.0%; $P = .001$; 48 hours after treatment, mean = 100.0% vs 12.2%, mean difference = 87.8%, 95% CI = 54.9% to 120.7%, $P < .001$; 72 hours after treatment, mean = 108.8% vs 10.4%, mean difference = 98.4%, 95% CI = 41.5% to 155.4%, $P = .002$) (Figure 8, B).

We next analyzed the effect on anchorage-dependent cell proliferation when niclosamide treatment was discontinued. Cell proliferation of niclosamide-treated cells was reduced after 5 days of daily doses of 1 μM niclosamide compared with solvent-treated cells (Figure 8, C). After 5 days, solvent-treated control cells reached the maximum. Removal of niclosamide on day 5 did not reverse the inhibition of cell proliferation for the following 5 days when compared with continuously niclosamide-treated cells.

We further analyzed metastasis formation in vivo under continuous and discontinuous niclosamide treatment. Mice were intrasplenically transplanted with HCT116-CMVp-LUC cells, and overall survival was analyzed in the solvent-treated control group (n = 6 mice), in the group that was continuously treated with daily doses of 20 mg/kg niclosamide (n = 6 mice), and in the group that

Figure 8 (continued).

imaging was performed. Exposure time was 1 second. Signal intensity of grayscale images (256 scale) were color coded (order of low to high signal intensity: **blue**, **green**, **yellow**, **red**, and **white**) and overlayed with bright field picture. Scale bar = 1 cm. **F**) S100A4 mRNA expression in spleen tumors from mice (n = 6 per group) treated as in panel (**D**). Tumor tissue was cryosected for RNA isolation. S100A4 mRNA level was measured by qRT-PCR and expressed as percent of control mice. The means and 95% confidence intervals of six experiments are presented. *P* values were calculated using two-sided one-way analysis of variance (ANOVA) and Bonferroni post hoc multiple comparison tests. **G**) Liver metastases of mice (n = 6 per group), treated as in panel (**D**), were quantified by scoring and expressed as percent of control mice. The means and 95% confidence intervals of six independent experiments are presented. *P* values were calculated using two-sided one-way ANOVA and Bonferroni post hoc multiple comparison tests. IB = immunoblot.

was treated with daily doses of 20 mg/kg niclosamide for 24 days and subsequently niclosamide treatment was discontinued (n = 6 mice). The overall survival increased in niclosamide-treated mice compared with solvent-treated mice (control vs discontinuous treatment, median survival = 24 vs 46.5 days, ratio = 0.52, 95% CI = 0.19 to 0.84, $P = .001$; control vs continuous treatment, median survival = 24 vs 43 days; ratio = 0.56, 95% CI = 0.24 to 0.88, $P = .001$) (Figure 8, D). Furthermore, no difference in overall survival was observed in mice treated with continuous vs discontinuous niclosamide treatment ($P > .05$).

On the individual endpoint of each mouse, liver and spleen were removed, and in vivo luminescence imaging was performed. All mice developed a spleen tumor at their individual endpoint. However, tumor growth in mice treated continuously or discontinuously with niclosamide was reduced compared with solvent-treated mice (Figure 8, E). The size of liver metastases in mice treated continuously or discontinuously with niclosamide was highly reduced compared with solvent-treated mice (Figure 8, E). In mice treated discontinuously with niclosamide, liver metastases were slightly larger compared with mice treated continuously with niclosamide. However, the luminescence signals from liver metastases of solvent-treated control mice were stronger on day 29 than the signal of liver metastases in mice treated continuously or discontinuously with niclosamide on day 50 (Figure 8, E), indicating a long-term inhibition of metastasis formation by niclosamide.

Quantification of the S100A4 mRNA level in the spleen tumor tissue by qRT-PCR showed that in niclosamide-treated mice, the S100A4 mRNA was reduced (control vs discontinuous treatment, mean = 100.0% vs 60%, mean difference = 40.0%, 95% CI = 3.9% to 50.1%, $P < .001$; control vs continuous treatment, mean = 100.0% vs 73%, mean difference = 27%, 95% CI = 15.8% to 64.2%, $P < .05$) (Figure 8, F). Moreover, no statistically significant difference in the S100A4 mRNA expression level was detected in mice with continuous vs discontinuous niclosamide treatment (discontinuous vs continuous treatment, mean = 60% vs 73%, mean difference = −13%, 95% CI = −37.2% to 11.2%, $P > .05$). Consistent with this result, the liver metastasis score was reduced in niclosamide-treated mice compared with control mice (control vs discontinuous treatment, mean = 100.0% vs 34.9%, mean difference = 65.1%, 95% CI = 18.4% to 111.9%, $P < .01$; control vs continuous treatment, mean = 100.0% vs 10.9%, mean difference = 89.1%, 95% CI = 45.3% to 133.0%, $P < .001$) (Figure 8, G). No statistically significant difference was observed in mice with continuous vs discontinuous niclosamide treatment (discontinuous vs continuous treatment, mean = 34.9% vs 10.9%, mean difference = 24%, 95% CI = −24.6% to 72.6%, $P > .05$) (Figure 8, G). In summary, these results showed that even when niclosamide was not continuously given, S100A4 expression, and metastases formation were highly inhibited leading to an increased overall survival.

Discussion

In this study, we performed a high-throughput screening of a library of 1280 compounds for identification of S100A4 transcription inhibitors. We used a colon cancer cell line expressing luciferase reporter gene whose expression was regulated by the S100A4 promoter to screen the library and identified niclosamide as the most efficient inhibitor of S100A4 promoter activity. We found that niclosamide inhibited the constitutively active WNT/CTNNB1 pathway signaling by inhibiting the formation of CTNNB1/TCF transcription activating complex at the S100A4 promoter; thus inhibiting the expression of S100A4 at the transcription level. Niclosamide-treated colon cancer cells showed reduced S100A4 mRNA and protein levels in a concentration- and time-dependent manner. Inhibition of S100A4 expression by niclosamide also showed inhibited S100A4-induced migration, invasion, proliferation, and colony formation of colon cancer cells in vitro. Moreover, we observed a novel antimetastatic function of niclosamide, because treatment with niclosamide reduced liver metastasis formation in mice bearing xenografted intrasplenic tumors. S100A4 expression was highly inhibited in tumors of niclosamide-treated mice. Furthermore, niclosamide-induced inhibition of metastasis formation was noted even 26 days after discontinuation of the treatment; thus showing a long-term effect. Increased overall survival of niclosamide-treated mice carrying the tumor xenografts was also noted.

Niclosamide is an antihelminthic drug that can be hydrolytically cleaved by cells of the gastrointestinal tract (26). Metabolism of niclosamide by tumor cells may explain our observation that small changes in the niclosamide structure could no longer inhibit S100A4 expression in vitro. Variation in aqueous solubility may be an additional factor underlying this structure-specific activity. Moreover, we found that the time-dependent reduction of S100A4 expression in vitro after a single dose of niclosamide treatment was restricted to 24 hours after treatment. This restriction could also be a result of a possible metabolization of niclosamide. To overcome this limited inhibitory action of niclosamide on S100A4 expression, we used daily doses of niclosamide to achieve a steady reduction of S100A4 expression, both in vitro and in vivo. Once this steady reduction level was reached, niclosamide-induced inhibition of S100A4 expression along with inhibition of cell motility and proliferation were stable, even after niclosamide treatment was discontinued.

Inhibition of S100A4 expression by short hairpin RNA or overexpression of endogenous inhibitors such as phospholipase A2, group IIA (PLA1G2A, platelets, synovial fluid) or interferon-γ results in reduced cell motility and invasiveness (27–29). Consistent with this result, niclosamide treatment of colon cancer cells showed decreased cell migration as well as invasion in our study, and inhibition of cell migration and invasion was overcome by ectopic overexpression of S100A4. Together, these observations emphasize the central role of S100A4 in cell motility leading to colon cancer metastasis.

It was previously observed in studies using RNA interference that reduction of the S100A4 expression level resulted in a G2/M arrest of pancreatic cancer cells and suppressed proliferation rates in gastric cancer cells (30,31). We observed that niclosamide treatment resulted in a reduction of S100A4 expression and a simultaneous reduction in cell proliferation. However, these two effects seemed to be independent, because ectopic overexpression of S100A4 could not overcome the antiproliferative effect of niclosamide. Recently, several studies reported antiproliferative effects of niclosamide in other cell systems and presented mechanisms that might be applicable to our findings (32–34). For

example, in acute myelogenous leukemia cells, niclosamide-induced generation of reactive oxygen species and subsequently apoptosis (32). Thus, apoptosis could be a possible mechanism responsible for the antiproliferative effect on niclosamide on colon cancer cells.

A recently published study in osteosarcoma cells demonstrated that niclosamide inhibited WNT signaling by internalization of frizzled-1 and proteasomal degradation of CTNNB1 (34). We found that in colon cancer cells niclosamide-induced inhibition of WNT/CTNNB1 target gene expression. A central step in the activation of WNT/CTNNB1 target gene expression is the nuclear transition of CTNNB1. However, under niclosamide treatment, the nuclear transition of CTNNB1 was not blocked indicating that the inhibition of WNT/CTNNB1 target gene transcription occurred downstream in the pathway. This indication was supported by EMSA and ChIP experiments used to analyze the formation of the CTNNB1/TCF complex. In those experiments, CTNNB1, though present at high levels in the nucleus, did not bind to TCF when cells were treated with niclosamide. Therefore, we suggest that in colon cancer cells niclosamide treatment inhibits CTNNB1/TCF complex formation and thereby interrupts target gene transcription.

Mutation of the WNT pathway is a fundamental step for colon cancer development leading to constitutive pathway activity and target gene expression (35). To date, few reports exist on WNT pathway inhibitors that target downstream of CTNNB1 to switch off the constitutively active signaling (36). We demonstrate that niclosamide represses the WNT signaling pathway despite the presence of mutated CTNNB1. WNT pathway activity in niclosamide-treated HCT116 and HAB-68^{mut} cells was reduced to the level of nonconstitutive activity found in HAB-92^{wt} cells.

WNT pathway activity plays a central role in colon homeostasis (37). Interference with this pathway therefore bears the risk of unwanted side effects (38). Niclosamide as a Food and Drug Administration (FDA)–approved drug is used in the clinic to treat helminthosis where it proved to have only slight side effects in humans when taken orally (39). In xenograft mouse models we found nontoxic concentrations that were effective in reducing the S100A4 expression level within the tumor tissue and substantially reducing liver metastasis. Interestingly, the inhibitory action of discontinued niclosamide treatment in vivo was nearly as strong as found in mice continuously treated with niclosamide. Despite discontinuation of niclosamide treatment, the S100A4 expression in the spleen tumor as well as the formation of liver metastases was inhibited for another 26 days after treatment discontinuation. Moreover, discontinued niclosamide treatment still had a major effect on the prolongation of overall survival.

This study has a few limitations. In the xenograft model, colon cancer cells were intrasplenically injected and niclosamide treatment occurred intraperitoneally. The researchers were not blinded to the groups, which bears the risk of biased result interpretation. Moreover, we only tested intraperitoneal, but not oral or intravenous application of niclosamide. Although niclosamide is an FDA-approved drug that is given orally to helminthosis patients, it needs to be further elucidated whether the amount of absorbed niclosamide is sufficient to establish an antimetastatic function in colon cancer patients. Moreover, the possibility of systemic intravenous application of niclosamide needs to be further investigated before niclosamide could be applied as antimetastatic drug in the clinic.

In conclusion, our current study presents niclosamide as a novel inhibitor of CTNNB1/TCF interaction that impairs S100A4 expression and thus S100A4-induced metastasis. S100A4 expression in tumors from colon cancer patients was shown to be prognostic for the development of metastases (4,7). Furthermore, we have recently shown that quantitative S100A4 transcript determination in plasma of colon cancer patients is prognostic and diagnostic for early cancer staging and defining patients at high risk for S100A4-induced metastases (40). Therefore, we conclude that the novel antimetastatic function of niclosamide bears great potential for the clinical treatment or prevention of colon cancer metastasis.

References

1. Nelson RS, Thorson AG. Colorectal cancer screening. *Curr Oncol Rep.* 2009;11(6):482–489.
2. Jemal A, Siegel R, Xu J, Ward E. Cancer statistics, 2010. *CA Cancer J Clin.* 2010;60(5):277–300.
3. Giles RH, van Es JH, Clevers H. Caught up in a Wnt storm: Wnt signaling in cancer. *Biochim Biophys Acta.* 2003;1653(1):1–24.
4. Stein U, Arlt F, Walther W, et al. The metastasis-associated gene S100A4 is a novel target of beta-catenin/T-cell factor signaling in colon cancer. *Gastroenterology.* 2006;131(5):1486–1500.
5. Helfman DM, Kim EJ, Lukanidin E, Grigorian M. The metastasis associated protein S100A4: role in tumour progression and metastasis. *Br J Cancer.* 2005;92(11):1955–1958.
6. Kim JH, Kim CN, Kim SY, et al. Enhanced S100A4 protein expression is clinicopathologically significant to metastatic potential and p53 dysfunction in colorectal cancer. *Oncol Rep.* 2009;22(1):41–47.
7. Gongoll S, Peters G, Mengel M, et al. Prognostic significance of calcium-binding protein S100A4 in colorectal cancer. *Gastroenterology.* 2002;123(5):1478–1484.
8. Ambartsumian NS, Grigorian MS, Larsen IF, et al. Metastasis of mammary carcinomas in GRS/A hybrid mice transgenic for the mts1 gene. *Oncogene.* 1996;13(8):1621–1630.
9. Davies MP, Rudland PS, Robertson L, Parry EW, Jolicoeur P, Barraclough R. Expression of the calcium-binding protein S100A4 (p9Ka) in MMTV-neu transgenic mice induces metastasis of mammary tumours. *Oncogene.* 1996;13(8):1631–1637.
10. Grum-Schwensen B, Klingelhofer J, Berg CH, et al. Suppression of tumor development and metastasis formation in mice lacking the S100A4(mts1) gene. *Cancer Res.* 2005;65(9):3772–3780.
11. Boye K, Maelandsmo GM. S100A4 and metastasis: a small actor playing many roles. *Am J Pathol.* 2010;176(2):528–535.
12. Kriajevska MV, Cardenas MN, Grigorian MS, Ambartsumian NS, Georgiev GP, Lukanidin EM. Non-muscle myosin heavy chain as a possible target for protein encoded by metastasis-related mts-1 gene. *J Biol Chem.* 1994;269(31):19679–19682.
13. Li ZH, Bresnick AR. The S100A4 metastasis factor regulates cellular motility via a direct interaction with myosin-IIA. *Cancer Res.* 2006;66(10):5173–5180.
14. Li ZH, Spektor A, Varlamova O, Bresnick AR. Mts1 regulates the assembly of nonmuscle myosin-IIA. *Biochemistry.* 2003;42(48):14258–14266.
15. Kriajevska M, Fischer-Larsen M, Moertz E, et al. Liprin beta 1, a member of the family of LAR transmembrane tyrosine phosphatase-interacting proteins, is a new target for the metastasis-associated protein S100A4 (Mts1). *J Biol Chem.* 2002;277(7):5229–5235.
16. Ambartsumian N, Klingelhofer J, Grigorian M, et al. The metastasis-associated Mts1(S100A4) protein could act as an angiogenic factor. *Oncogene.* 2001;20(34):4685–4695.
17. Mathisen B, Lindstad RI, Hansen J, et al. S100A4 regulates membrane induced activation of matrix metalloproteinase-2 in osteosarcoma cells. *Clin Exp Metastasis.* 2003;20(8):701–711.

18. Saleem M, Kweon MH, Johnson JJ, et al. S100A4 accelerates tumorigenesis and invasion of human prostate cancer through the transcriptional regulation of matrix metalloproteinase 9. *Proc Natl Acad Sci U S A.* 2006; 103(40):14825–14830.
19. Yammani RR, Carlson CS, Bresnick AR, Loeser RF. Increase in production of matrix metalloproteinase 13 by human articular chondrocytes due to stimulation with S100A4: role of the receptor for advanced glycation end products. *Arthritis Rheum.* 2006;54(9):2901–2911.
20. Kim JS, Crooks H, Dracheva T, et al. Oncogenic beta-catenin is required for bone morphogenetic protein 4 expression in human cancer cells. *Cancer Res.* 2002;62(10):2744–2748.
21. Hernan R, Fasheh R, Calabrese C, et al. ERBB2 up-regulates S100A4 and several other prometastatic genes in medulloblastoma. *Cancer Res.* 2003; 63(1):140–148.
22. Engelkamp D, Schafer BW, Erne P, Heizmann CW. S100 alpha, CAPL, and CACY: molecular cloning and expression analysis of three calcium-binding proteins from human heart. *Biochemistry.* 1992;31(42):10258–10264.
23. Rapisarda A, Uranchimeg B, Scudiero DA, et al. Identification of small molecule inhibitors of hypoxia-inducible factor 1 transcriptional activation pathway. *Cancer Res.* 2002;62(15):4316–4324.
24. Sekine S, Shibata T, Sakamoto M, Hirohashi S. Target disruption of the mutant beta-catenin gene in colon cancer cell line HCT116: preservation of its malignant phenotype. *Oncogene.* 2002;21(38):5906–5911.
25. Sherbet GV. Metastasis promoter S100A4 is a potentially valuable molecular target for cancer therapy. *Cancer Lett.* 2009;280(1):15–30.
26. Espinosa-Aguirre JJ, Reyes RE, Cortinas de Nava C. Mutagenic activity of 2-chloro-4-nitroaniline and 5-chlorosalicylic acid in Salmonella typhimurium: two possible metabolites of niclosamide. *Mutat Res.* 1991; 264(3):139–145.
27. Kim TH, Kim HI, Soung YH, Shaw LA, Chung J. Integrin (alpha6beta4) signals through Src to increase expression of S100A4, a metastasis-promoting factor: implications for cancer cell invasion. *Mol Cancer Res.* 2009;7(10):1605–1612.
28. Ganesan K, Ivanova T, Wu Y, et al. Inhibition of gastric cancer invasion and metastasis by PLA2G2A, a novel beta-catenin/TCF target gene. *Cancer Res.* 2008;68(11):4277–4286.
29. Andersen K, Smith-Sorensen B, Pedersen KB, et al. Interferon-gamma suppresses S100A4 transcription independently of apoptosis or cell cycle arrest. *Br J Cancer.* 2003;88(12):1995–2001.
30. Tabata T, Tsukamoto N, Fooladi AA, et al. RNA interference targeting against S100A4 suppresses cell growth and motility and induces apoptosis in human pancreatic cancer cells. *Biochem Biophys Res Commun.* 2009; 390(3):475–480.
31. Hua J, Chen D, Fu H, et al. Short hairpin RNA-mediated inhibition of S100A4 promotes apoptosis and suppresses proliferation of BGC823 gastric cancer cells in vitro and in vivo. *Cancer Lett.* 2010;292(1):41–47.
32. Jin Y, Lu Z, Ding K, et al. Antineoplastic mechanisms of niclosamide in acute myelogenous leukemia stem cells: inactivation of the NF-{kappa}B pathway and generation of reactive oxygen species. *Cancer Res.* 2010; 70(6):2516–2527.
33. Balgi AD, Fonseca BD, Donohue E, et al. Screen for chemical modulators of autophagy reveals novel therapeutic inhibitors of mTORC1 signaling. *PLoS One.* 2009;4(9):e7124.
34. Chen M, Wang J, Lu J, et al. The anti-helminthic niclosamide inhibits Wnt/Frizzled1 signaling. *Biochemistry.* 2009;48(43):10267–10274.
35. Fearon ER, Vogelstein B. A genetic model for colorectal tumorigenesis. *Cell.* 1990;61(5):759–767.
36. Sack U, Stein U. Wnt up your mind—intervention strategies for S100A4-induced metastasis in colon cancer. *Gen Physiol Biophys.* 2009;28:F55–F64. Focus Issue.
37. Radtke F, Clevers H. Self-renewal and cancer of the gut: two sides of a coin. *Science.* 2005;307(5717):1904–1909.
38. Barker N, Clevers H. Mining the Wnt pathway for cancer therapeutics. *Nat Rev Drug Discov.* 2006;5(12):997–1014.
39. Merschjohann K, Steverding D. In vitro trypanocidal activity of the anti-helminthic drug niclosamide. *Exp Parasitol.* 2008;118(4):637–640.
40. Stein U, Burock S, Herrmann P, et al. Diagnostic and prognostic value of metastasis inducer S100A4 transcripts in plasma of colon, rectal, and gastric cancer patients. *J Mol Diagn.* 2011;13(2):189–198.

Funding

German Research Association (STE 671/8-1 to USt and PMS), the Alexander von Humboldt Foundation (to USt and WW), and the Max-Delbrück-Center for Molecular Medicine Helmholtz Association fellowship (to USa).

Notes

We are very grateful to Pia Hermann and Jutta Aumann for their technical assistance and to Franziska Siegel and Mathias Dahlmann for their methodological and scientific advice. The authors are solely responsible for the design of the study, the analysis and interpretation of the data, the writing of the article, and the decision to submit the article for publication.

Affiliations of authors: Max-Delbrück-Center for Molecular Medicine (USa, DK, ML, IF), Experimental and Clinical Research Center, Charité University Medicine at the Max-Delbrück-Center for Molecular Medicine (USt, WW), Berlin, Germany; Screening Technology Branch, Developmental Therapeutics Program, Division of Cancer Treatment and Diagnosis, National Cancer Institute-Frederick, Frederick, MD (DS, MS, RHS); Charité Comprehensive Cancer Center, Charité University Medicine, Berlin, Germany (PMS).